PEELING AND TORSIONAL SHEAR OF PORCINE THORACIC AORTA

A Thesis

by

AKSHAY RAGHAVENDRA RAO

Submitted to the Office of Graduate and Professional Studies of
Texas A&M University
in partial fulfillment of the requirements for the degree of

MASTER OF SCIENCE

Chair of Committee,	Chandler Benjamin
Co-Chair of Committee,	K.R. Rajagopal
Committee Member,	Michael Moreno
Head of Department,	Andreas A. Polycarpou

May 2019

Major Subject: Mechanical Engineering

ABSTRACT

Peeling of the aorta is a phenomenon with particular relevance for cardiovascular diseases like aortic dissection. There is initiation of a tear and then delamination between the medial layers. The tear can propagate into the body cavity or back into the artery creating a secondary flow. The tear can be circumferential, axial or in any direction. It usually occurs in the Thoracic aorta. Previous experimental studies have obtained the response under these conditions for human aorta samples in an attempt to obtain a peeling energy. Reasons for the initiation of the tear are currently poorly understood but insight into its propagation is a step forward. Measuring the peeling energy required for the tear to propagate improves our understanding of the condition. A technique is presented to measure the stretch undergone by the arms by optically tracking microspheres adhered to the arms. Accurate measurement of the stretch could lead to better peel energy calculations. Here, a protocol is described for measuring delamination energy in porcine aortas as a first step towards measuring delamination energy in healthy and diseased human aortas.

Aortic tissue can undergo shearing deformation in physiological conditions like the twisting of the head for carotid artery. It is accepted that wall shear stresses control the production of many active molecules from the endothelial cells. Experimental data is needed for constitutive models which include the shearing behavior of the arterial wall. Unfortunately most experimental data is related to extensional behavior even. As such torsional shearing of the aorta wall at high amplitudes as well as the effect of shear rate is looked into.

Finally the dynamic response of the arterial wall is investigated. Arterial tissue is known to exhibit creep under constant load and relaxation under a constant strain.

The arteries also undergo cyclic hemodynamic loading and procedures like balloon angioplasty require an understanding of the time dependent response. There is an initial investigation into the creep and relaxation behavior under torsional shear at high strains.

ACKNOWLEDGEMENTS

Thank you Mummy, Appa, Aishu and Adi for your constant nagging and support. Thank you my dear friends and fellow colleagues with whom I have been lucky to share my experiences.

Thank you Dr. Benjamin and Dr. Rajagopal for supporting me along my research. Without your patience and guidance I would still be at my first cross roads.

I'd also like to thank TEES for funding this project without which this would not be possible.

"Look up at the enormous sky and see the starshine.

See the world in a light with all its darkness."

CONTRIBUTORS AND FUNDING SOURCES

Contributors

This work was supervised by a thesis committee consisting of Professor Chandler Benjamin [advisor] and K.R. Rajagopal [co advisor] of the Department of Mechanical Engineering and Professor Michael Moreno of the Department of Biomedical Engineering.

All work for the thesis was completed by the student, in collaboration with Manoj Myneni of the Department of Mechanical Engineering.

Funding Sources

This work was made possible in part by TEES of Texas A&M. Its contents are solely the responsibility of the authors and do not necessarily represent the official views of the TEES.

TABLE OF CONTENTS

Page

LIST OF FIGURES

FIGURE Page

LIST OF TABLES

TABLE Page

1. INTRODUCTION

1.1 Peeling Experiments and Failure Studies of Aorta

Understanding the fracture properties of aortic tissue are essential to understanding the failure of arteries in diseases like aortic dissection and aneurysms. Prior studies have investigated radial tensile strength and peeling energy [21, 32, 38, 24]. Other works look into biaxial mechanical properties of human dissected tissues [5] and use infused blebs and their propagation [6, 26, 12, 40, 36]. To help improve our understanding of cardiovascular diseases and develop effective treatments, understanding the mechanics of aortic tissue is essential.

Some of the first studies into peeling of aortic samples also include histological analysis. Maclean et al. [21] conducted experiments to study the radial elastic properties of aortas. Porcine tissue samples were cut from upper and lower segments of the thoracic aorta and were tested radially, circumferentially and longitudinally using a tensile testing machine. The elastic properties were compared under these loading conditions. The results indicated that radial Young's Modulus was much lower than either circumferential or longitudinal. Histological studies showed that there was a separation of elastin layers as strain was increased from 0 to 2.5.

Sommer et al. [32]worked on direct tension tests and peeling tests of 15 human Abdominal Aortas. Insight was gained into microscopic changes through histological studies at different peeling stages. Peeling in the axial direction exhibited a "rougher" dissection surface when compared to the circumferential direction. For the study 19 human abdominal aortas were harvested within 24hrs from death. Segments were taken from the infrarenal portion of the AA.

Two types of tests; namely Direct Tension and Peeling tests were performed.

The mechanical testing was carried out with the specimens immersed in a .9 % saline solution. For the peeling tests, the upper and lower clamps moved in opposite directions, keeping the specimen in place. For direct Tensile tests two plastic rods with sandpaper inside cylindrical recesses were used for the direct tensile test. The coin-shaped specimen was glued to the sandpaper using cyanoacrylate glue.

To study microstructural changes histology was conducted. These specimens were prepared specifically for histology. Accordingly, the specimens were not peeled to failure. Instead, they were peeled half way and a special specimen holder was designed to maintain this loading state.

Histological mages indicated that the peeling in the axial direction created "rougher" surfaces compared to circumferential. Dissection in circumferential direction propagated between elastic laminae while in axial direction it crossed them. This might show the anisotropic nature of the human AA.

The tissue appeared to be linear elastic in the radial direction while having a force-displacement plateau for peeling. One of the main suggestions of the work is that the dissection properties seem to be anisotropic, but is limited by the number of specimens tested. More studies are required before ascertaining anisotropic properties of the human aorta. We can see **??** for some representative results.

Testing diseased as well as healthy tissues under peeling and carrying out comparisons can help improve our understanding of the effect of atherosclerotic plaque formation on the mechanical response.

Tong et al. [38] looked into the dissection properties of 31 pairs of human carotid arteries and conducted direct tension and peeling tests. The specimens were both healthy as well as diseased(atherosclerotic). It was seen that the interface between the healthy adventitia and media had the highest radial failure stress. The force/width values to separate individual layers were smaller for the circumferential direction

compared to the axial direction. Dissection energies per reference area generated during the peeling tests were also lower for the strips in the circumferential direction compared to the axial direction and varied with location. Histology showed that interfacial ruptures occur mostly in the media and 2-5 elastic lamellae away from the internal and external elastic laminae. Direct tension tests were of two types. One with healthy tissues in the media, the interface of the media and intima(I+M) and the interface between the media and the adventitia. And the other with diseased tissue with atherosclerotic plaque where the adventitia was removed. It was not possible to separate the intima and the media. To control the initiation, the coin-shaped specimens were cut with a circumferential incision of 1mm depth. For peeling tests, rectangular strips of about 18.0mmx6.0mm were cut. Again an initial cut was given to help control propagation. Peeling of diseased specimens was not conducted as controlled propagation was very difficult.

In addition to peel experiments, other modes of deformation are necessary to get a more complete idea of the behavior. [5] Babu et al. looked into the biaxial mechanical properties of human type A dissections and a microstructurally motivated strain energy function. The results indicated higher stiffness for dissected tissues compared to healthy control aortas. There was no apparent correlation between stiffness and higher aortic diameter or age of the patient. Specimens were stored in Dulbecco's saline at 4 C supplemented with sodium nitroprusside to passivate smooth muscle cells.

Tests were conducted on a biaxial reactor and strains were measured with the help of an overhead camera and MATLAB algorithm to track graphite markers. The specimens were attached to the linear actuators using fish hooks with suture threads. Cauchy stress and green strain were calculated and tissues gave a nonlinear response. Most specimens also showed anisotropic response with increased stiffness

in the longitudinal direction. Transition points from elastin dominated to collagen dominated behavior were determined for the tests.

To study the response of the various components of the aortic tissue it is possible to apply enzymes to break down the tissue selectively. [23] Noble et al. looked into the effects of elastase, glutaraldehyde, and collagenase on the response of porcine aorta to peel testing. They suggested that the resistance to dissection can be quantified by the critical energy release rate. These treatments are used here to model diseased tissue.

Sherifova et al. [29] performs a wide range of experimental tests aimed at modeling the propagation of aortic dissection. The Tsai-Wu failure criterion is used to obtain the failure surface. The aorta wall was taken as a three-layered fiber reinforced material. Uniaxial tests in circumferential, radial and longitudinal along with shear tests are performed to obtain the failure criteria coefficients.

In addition to peel experiments to study the fracture behavior of aortic tissue, bleb based studies have also been conducted on samples. For this a small incision is made and a bleb is created and slowly propagated using a syringe and ink as fluid. [6] Carson et al. attempted to understand the mechanical strength of the media and study aortic propagation by experimental studies. They infused a bleb of India ink while continuously recording the pressure to determine the peak hydraulic pressure the media can withstand, the distensibility of the aorta and to estimate the wall stresses.

For the experiment, porcine descending thoracic aortas are harvested and maintained in an isotonic solution. It is cut to form a rectangular slab. A needle is then inserted into the center of the media. Using illumination by a fiber optic cable, a video camera and pressure transducer they kept track of the projected area of the bleb and pressure measurements. A volume of India ink diluted with an isotonic

solution was injected into the tunica media sing a syringe pump. A successful experiment meant a bleb was formed and so a tear would propagate. After the experiment, the bleb was sliced open and the depth of the bleb was recorded as a percentage of wall thickness. A maximum of 4 blebs per aorta was decided and it was also determined that infusion rate did not have a noticeable effect on the experiment. Two test regions were determined, below the arch and upper thoracic.

It was assumed that peak hydraulic pressure was related to medial strength. The pressure-volume curves obtained had a few distinct regions. An initial linear portion where pressure rises with not much change in volume. The slope of this region was calculated as the distensibility of the media. And there was a region where the pressure drops and the bleb volume increases representing the propagation of the tear.

To calculate distensibility it was assumed that the aorta is composed of incompressible tissue, the fluid infused into the media forms a sphere and the aorta expanded into the surrounding space as fluid was infused into the media.

The work of dissection was the area under the P V curve. The pressure was integrated sequentially over the volumes of the bleb.

One issue with the calculated distensibility is in determining the initial volume. No relationship was found between P max and tear depth. Peak pressure was found to be much higher than physiological pressure. As the pressure drops after the tear has formed, this indicates that pressure for the propagation of the tear is low.

For distensibility, it was determined that the bleb is initially ellipsoidal and becomes spherical over time. Additionally, it was found that peak pressure, distensibility, area of the curve are all unrelated to the depth of the media. It is seen that the work of dissection does not change much after the dissection has started. They also attempt to calculate the vertical wall tensile stress using the pressure-volume data.

[37] Tiessen et al. aimed to study the initiation and propagation of a medial tear by measuring the pressure while infusing India ink at a constant flow rate into the middle of the media. Pressure-volume curves were obtained and used to calculate distensibility, work, and peak pressure. Correlations between these and sex, age, atherosclerotic formation, etc were investigated.

The experiment was conducted on 21 human aortas and results indicated that atherosclerosis may only alter the path of dissection and does not have an effect on required pressure.

[36] Tam et al. investigated the effect of tear depth on propagation pressure of an aortic dissection. Saline was injected to create a bleb inside the intimal side of the aortic wall. A circumferential slit was created connecting the false to the true lumen and then the aortas were pressurized statically until there was a propagation of the tear. Histological sections were used to determine the depth of the tear. It was found that propagation pressure depends on the number of elastin layers on the outer wall of the dissection and the tear depth.

Porcine specimen were obtained and aortas were harvested and tested within 48 hours of death. Blebs were created by injecting saline into the media. Then a circumferential tear was created from the intimal side. All of this was done after flipping the aortas inside out. Once everything was completed there were once again flipped right side out. The aortas were then cannulated, submerged in saline solution and pressurized under static conditions. India ink was used to help improve the visibility of the bleb. The pressure was same in the lumen and bleb, and it was increased until there was propagation in either the antegrade or retrograde direction. Aortas that were not pressure tight were discarded.

After the experiment, the specimens were fixed in 4 percent formaldehyde and sections were cut and stained for histology. The number of elastin layers on the outer

wall and intact wall was then counted. Tear depth was determined to be one minus the ratio of dissected layers to intact layers. A small value corresponds to an intimal flap while a value close to one represents a thick flap.

Propagation pressure was plotted vs number of layers in the dissected wall and vs tear depth. It was found that propagation pressure was linearly related to both tear depth and the number of dissected wall layers. This linear dependence was explained by suggesting that the thickness of the outer wall affects the stress distribution of the dissection. They later continue to discuss prior works and their relevance to this study.

It is concluded that the reported propagation pressure is possible in vivo conditions under certain situations that might affect the pressure vs tear depth curve like thrombus formation, hypertension, and connective tissue disorders like Marfan's syndrome.

1.2 Shearing of Aortic Tissue

Studying the mechanics of aortic tissue is a crucial component in understanding its behavior under healthy and diseased conditions. Wall shear stress and circumferential stress have been largely accepted as significant factors in arterial growth and remodeling as a response to changes in flow and pressure. But, experimental studies on aortic tissues have largely focused on uniaxial and biaxial tests which are more suited for investigating circumferential stress. This may be explained by the inherent convenience of gripping tissue and then applying deformations in the uniaxial and biaxial modes. As such, the behavior of aortic tissue under shear has been left relatively unstudied.

The difficulties that arise with shearing experiments on biological tissues have been investigated [18, 15]. Even so, there have been attempts at characterizing shear

behavior of biological materials like vocal fold tissue [41, 22, 27], brain tissue [30], adipose tissue [31] and liver tissue [3].

When it comes to shear characterization of cardiovascular tissue in particular, studies have been conducted to understand human myocardium specimen [34],rat myocardium [8] and pig myocardium [9] using a triaxial tester. [2] presented a general approach to study the mechanical behavior of soft materials by applying tensile, compressive or shear loads on a cuboidal myocardium specimen. On the other hand, aortic wall tissue has been rarely studied under shear loading. This is probably due to the inherent difficulties of conducting these experiments like specimen size and applying the different shear modes.

Some biaxial tests have been used to study the shear strains induced. Sommer et al. [33] conducted biaxial tests on 14 passive human myocardium specimen and investigated the shear stresses that can arise when performing these tests. Normal and shear stresses are determined. Strain quantification is improved by increasing the number of markers and using shape functions.

Sommer et al. [34] used a triaxial tester to study the shear properties of myocardium. Sinusoidal simple shear was applied with the specimen contained in a bath at 37 celsius. Afterwards, relaxation tests with .5 shear were performed to observe the viscoelastic properties. All tests were performed for all six shear modes. Specimen were cut as cubes with faces perpendicular to the three orthogonal axes along the myofiber direction, transverse to the fiber direction in the layer, and normal to the layers. Adhesive was used to fix the specimen and after testing specimens were checked for seepage of glue.

The difficulties that arise with rheological studies of biological tissue, especially solids may be a contributor to the sparsity of experiments. [18] Janmey et al. give a basic explanation of rheology principles followed by concerns to consider while de-

signing an experimental setup to study biological tissues. They discuss the special considerations to be considered for biological materials like their frailness, nonlinearity, and the small range of strains possible. Sacks [28] presents a review of techniques used for characterizing soft tissues. The progress from uniaxial to biaxial and finally triaxial tests is discussed along with the difficulties of integrating the constitutive model with the experimental test. Horgan et al[15] review the challenges in conducting simple shear experiments and in obtaining the parameters for constitutive models. Simple shear of fibre reinforced elastic materials, shear response for soft tissues, the effects of fiber orientation, shear stress on inclined faces and normal stress response are discussed along with the past attempts to address these issues.

The authors mention the difficulties in studying biological tissues like how tissues undergo biochemical changes after isolation and storing. Another major issue is the heterogeneity of tissues. They are multilayered, consisting of many cell types each with its own mechanical properties, orientation, and strength. Although it is mentioned that there are materials in use today that exhibit similar levels of complexity like carbon fiber composites.

Sommer et al. [31] conducted biaxial tests and triaxial shear tests on human adipose tissue. For the triaxial shear tests, the specimen were affixed with the help of adhesive and tests were carried out in a physiological solution. Shear was applied sinusiodally in orthogonal directions for all six modes of shear. After the shear tests, relaxation tests were conducted at 0.5 shear strain.

The results indicated the behavior was anisotropic while previous studies where adipose tissue was treated as isotropic,nonlinear,and viscoelastic.

[22] Miri et al study the anisotropic elastic properties of vocal fold tissue. A linear transversely isotropic model is used. Experimental studies is conducted by traction testing along with shear rheometry.

Porcine vocal fold lamina is noted to be single layered. A circular disk was cut out from the sample while attempting to maintain a uniform thickness. For rheometric testing, the initial thickness of the specimen was measured using a caliper. Then a parallel plate configuration was used to apply oscillation tests in a stress-controlled mode over a certain frequency range with a constant normal force. Normal force application was noted to improve the consistency of shear modulus results.

One axis of anisotropy was used which gives five independent constants required for the transversely anisotropic model which has been used before extensively for vocal fold tissue.

Six sets of porcine fold tissue are subjected to rheometric testing. From this the longitudinal and two defined shear modulus are obtained. It is proposed that anisotropy is due to the orientation of collagen fibrils (an extracellular protein) in the longitudinal direction. The study also includes traction experiments but it is not discussed here.

[27] Rohfls et al. suggest a novel technique to study the anisotropic viscoelastic properties of vocal fold tissue. They devised an experimental method to apply shear stress in a given direction. In addition histological staining is conducted and the orientation of collagen fibers is looked into. It is concluded that the transverse and longitudinal shear response is different.

For the testing, a linear skin rheometer is modified to apply shear stress in a given direction. The probe is attached via a suction cup to the vocal fold epithelium. A sinusoidal force is then applied and the displacement is recorded.

Shuck et al. [30] characterize the shear response of brain tissue using a torsional rheometer to shed light on the response during head injury impacts. The linear viscoelastic properties are determined using a four-parameter model. Failure criteria are studied based on maximum shear strain and strain rate.

Abraham and others[1] carried out simple lap shear tests on bovine meniscal samples to study the effect of anatomical locations and fiber orientation on the response. The homogeniety of the deformation was checked using DIC techniques which found that there was some warping near the edges of surfaces and this is suggested to be due to penetration of adhesive. The meniscus was considered to be a isotropic matrix with orthogonal fiber families.

Avazmohammadi [2] et al. presented an approach for the characterization of biological materials that incorporates the chosen strain energy density function in deciding the experimental tests. An optimal set of displacement paths is chosen and then applied via a novel triaxial tester that can apply tensile, compressive, or shear loads on a cuboidal specimen of around 10mm dimensions. An inverse FEM simulation is used to estimate the parameters of the strain energy density function. The approach is validated using an isotropic elastomer as well as a transversely isotropic elastomer (isotropic urethane rubber is reinforced with thin steel needles). Post infarcated myocardium samples were tested. The displacement paths are optimized to reduce error and dependence of the parameters on the applied loading.

2. PEELING OF PORCINE THORACIC AORTA

2.1 Introduction

Peeling of the aorta is an important phenomenon with particular relevance for cardiovascular diseases like aortic dissection. Here there is initiation of a tear and then delamination between the medial layers. The tear can propagate into the body cavity or back into the artery creating a secondary flow. Previous experimental studies have obtained the response under these conditions for human aorta samples in an attempt to obtain a peeling energy. Here these studies are taken forward by using a technique to measure the stretch undergone by the peeled arms. Stretch is measured by optically tracking 200 300 μm microspheres adhered to the peeling halves. An improved measurement of this stretch could potentially lead to more accurate peeling energy calculations.

Measuring the stretch in the arms of the peeling specimen could give valuable insights into the nature of tearing of aortic tissue. There have been experiments to look into peeling energy calculations. These studies have assumed a linear relationship between the stress and stretch. The response of diseased and healthy tissue could vary widely. As such experimental studies have been compared their response. [24] Pasta et al. compared the dissection properties of aneurysmal and non-aneurysmal ascending thoracic aortas in humans. 31 aortic segments with and without ATAA (Ascending Thoracic Aortic Aneurysm) were studied.

[23] Noble et al. tested porcine aorta in circumferential and longitudinal directions.The specimens were then treated with the appropriate enzymes to test behavior of the aortic components.

The critical energy release rate (G) was determined by taking the difference of

external work done and elastic work by the specimen length. External work was calculated by multiplying mean tensile force with the elongated length while elastic work was obtained from the difference in lengths between initial and elongated. The inearity in constitutive response is assumed.

Other studies have observed the response under direct tension in the radial direction. Circular samples were punched out and tested radially to understand failure properties. Tong et al. [38] observed the dissection properties of 31 pairs of human carotid arteries and conducted direct tension and peeling tests. The specimens were both healthy as well as diseased(atherosclerotic).

Direct tension tests were of two types. One with healthy tissues in the media, the interface of the media and intima(I+M) and the interface between the media and the adventitia. And the other with diseased tissue with atherosclerotic plaque where the adventitia was removed. It was not possible to separate the intima and the media. Peeling of diseased specimens was not conducted as controlled propagation was very difficult.

The average force per unit width from the peeling test on the media was lower for the circumferential direction than the axial direction. Histological analysis indicated that the rupture occurred close to the interface. It was also apparent that peeling axial strips gave a rougher dissection surface than the axial direction. It showed that axial dissection crossed elastic layers while circumferential peeling occurred along the layers.

Some prior studies included histological analysis to confirm that the tear propagated only through the media. Sommer et al. [32] tested 15 human Abdominal Aortas and carried out histological studies at different peeling stages. Peeling in the axial direction exhibited a "rougher" dissection surface when compared to the circumferential direction. Direct Tension and Peeling tests were performed after sep-

arating the three layers using a surgical scalpel. Only the medial layer was used for the tests.

It is important to note that all prior tests have obtained average measurements of the stretch as well as the specimen dimensions. Measurement of the local properties could give us new information about the tearing phenomenon.

2.2 Methods

2.2.0.1 Specimen Harvest

Heart and aorta are collected from freshly killed hogs from a slaughterhouse on Texas A&M University campus. Samples are placed in an ice box for transportation to the lab. Using dissection tools, the aorta is separated from the heart and is cut into thoracic and abdominal segments. The thoracic aorta is further divided into upper descending and lower descending regions. These samples are stored at -20^{0}C in centrifuge tubes containing Phosphate buffer saline(PBS) solution.

2.2.1 Peeling

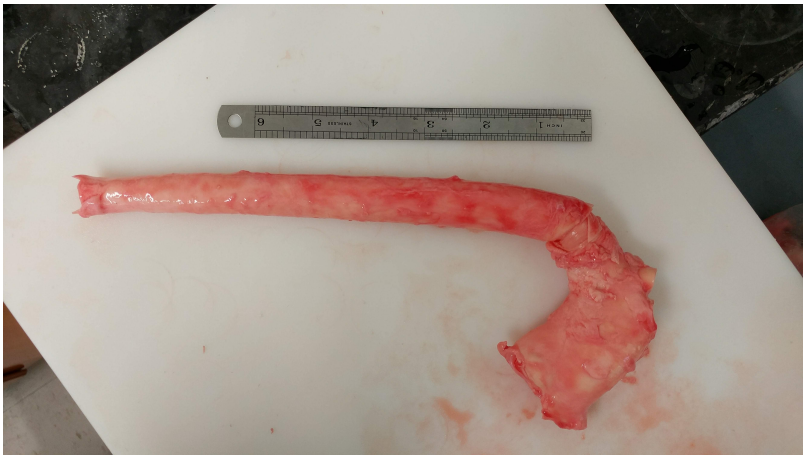

Figure 2.1: Cleaned Aorta

2.2.1.1 Specimen Preparation

On the day of experiments, frozen specimens which are stored at -20 C are thawed over a period of 12 hours at 0 C. Loose connective tissue is carefully removed without damaging the aortic layers. The aorta is cut and layed flat. Rectangular specimens are cut out from the tissue. Around 4 samples per segment in both descending and ascending aorta are obtained.The specimens are stored in PBS at 0 C until the time of testing. All specimens are tested within 4hrs of thawing.

Microspheres are carefully applied on either side of the samples on one face. An incision is created of appropriate depth. Incision is created using scalpel and then propagated manually to a certain length. Microspheres are touched to adhesive and carefully applied to specimen surfaces. Equal number on either side. With equal spacing. Microspheres are placed with enough distance between them that they do not come into contact while entering the peeling zone curvature but also such that there are enough spans for stretch measurement.

(a) The aorta cut into the regions (b) Rectangular Peel Specimens

Figure 2.2: Peel Specimen Preparation

2.2.1.2 Experimental Setup

The arms of the specimen are gripped tightly using stainless steel grippers with rough surfaces to prevent slipping of biological specimen. Once the arms are carefully held such that the microspheres are not disturbed, the grippers are mounted on a uniaxial testing apparatus. A CCD camera is placed directly above the specimen. Due to the camera placement not having much flexibility, a mirror was placed at a 45°angle as can be seen in 2.3a. A white background is installed to allow for contrast with the black microspheres. A sample image before the protocol has begun can be seen in in 2.3b. Images were checked for distortions to make sure that using the mirror would not introduce any errors. It was found to be less than 5%; please see 2.4a and 2.4b.

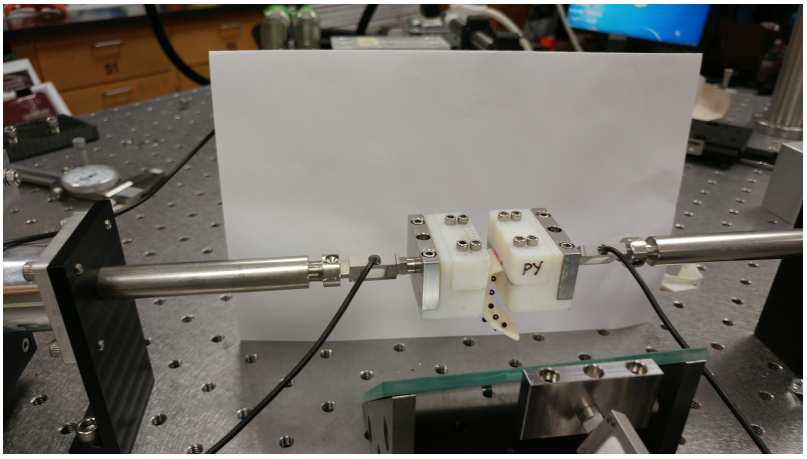

(a) Experimental Setup

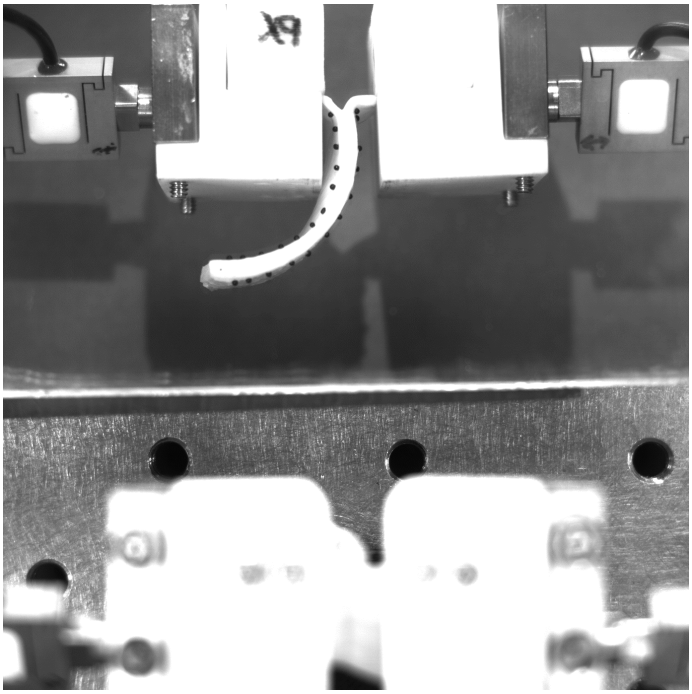

(b) Image Captured from CCD Camera

Figure 2.3: Experimental Setup

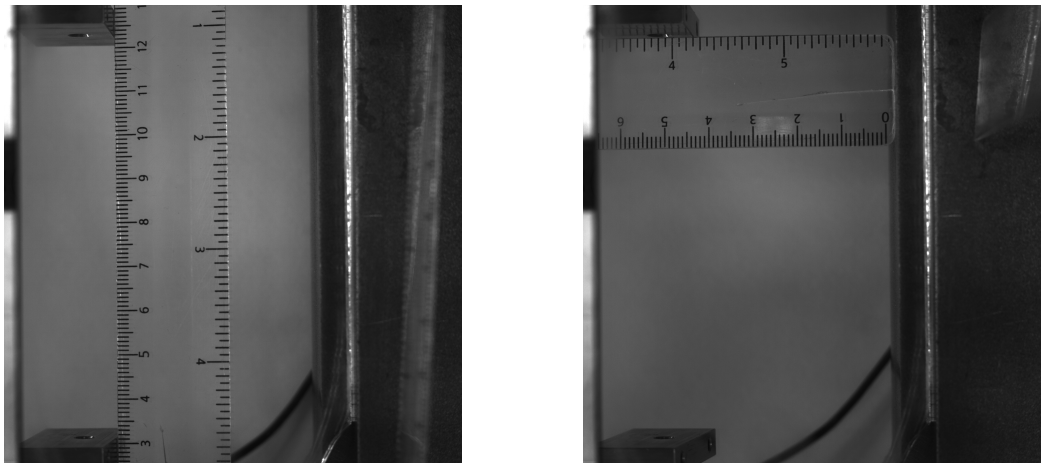

(a) Horizontal Distortions (b) Vertical Distortions

Figure 2.4: Check for Image Distortions from Mirror

2.2.1.3 Peel Images:Measuring Initial Distance

To measure the stretch we take the ratio of the distances between consecutive markers during the test to the distance between the same markers before initiation of the test see 2.5b. The initial distance between markers is measured as the linear distance in the first image. Before the spans are under stretch. We assume that the tissue is in a stress free configuration. Also, the markers are labelled according to their position for later analysis as can be seen in 2.5a.

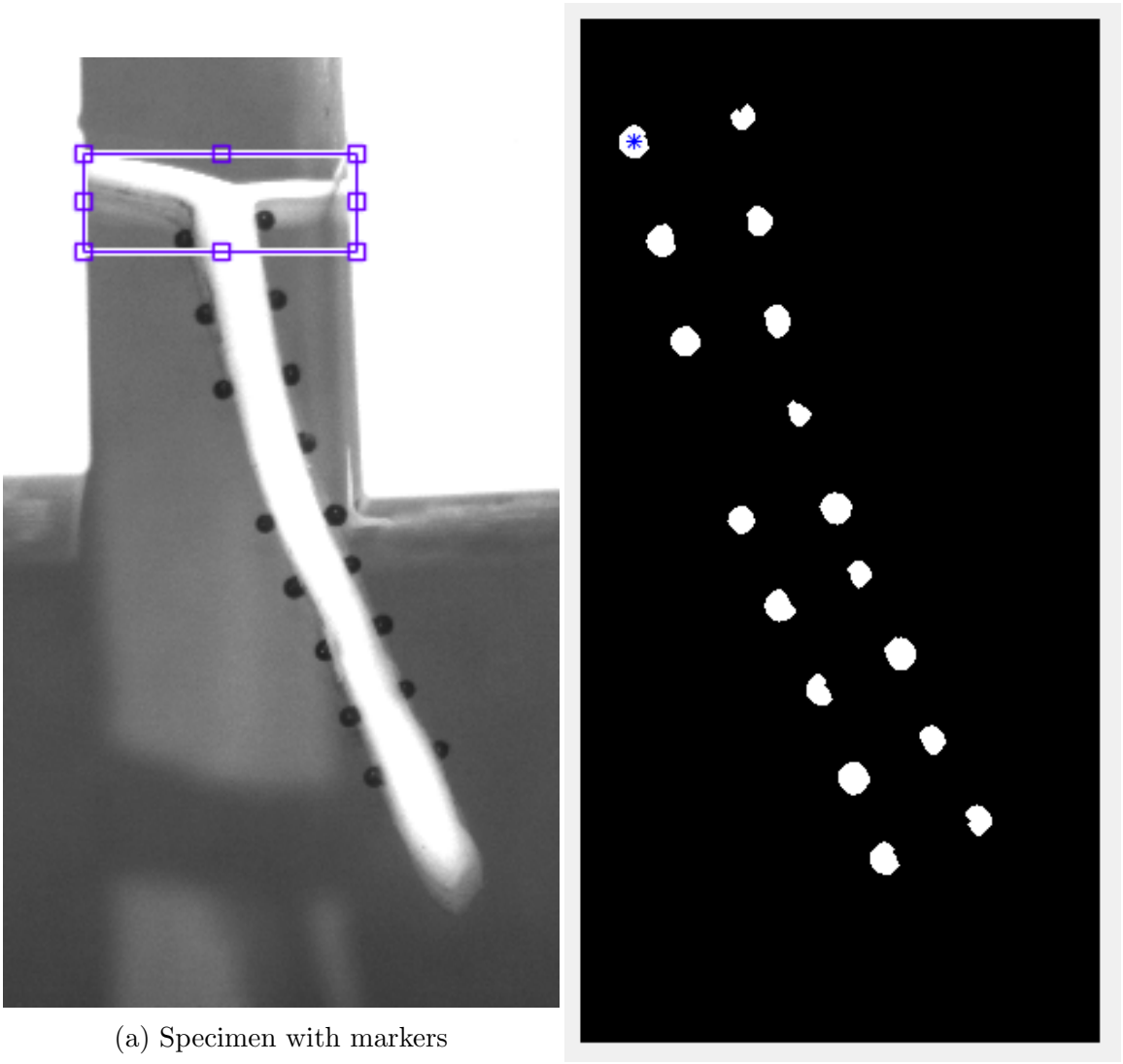

(a) Specimen with markers

(b) Markers after Applying Threshold

Figure 2.5: (a) Adventitial Specimen (b) Selecting Markers

2.2.1.4 Peel Images:Pre-processing

We choose an intial region of interest as can be seen in 2.6a. The height remains constant throughout the test. The width of the region of interest continues to increase according to the rate of movement of the gripping arms.

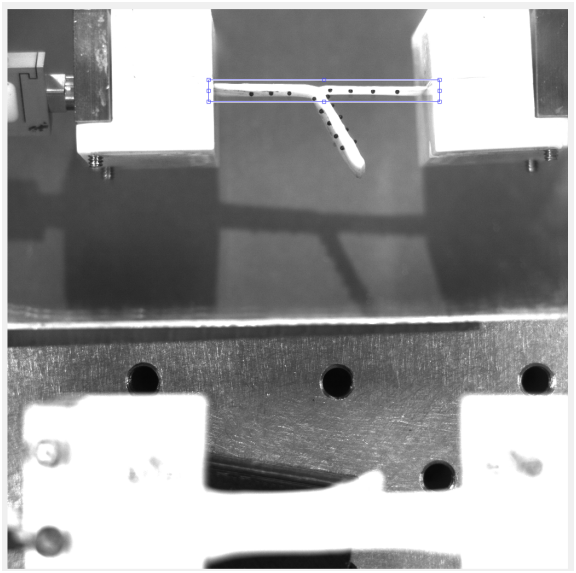

(a) Selecting a region of interest

(b) Checking Processing

Figure 2.6: ROI and Preprocessing Filters

The image must be processed with various filters to identify the markers. First we apply a thresholding filter whose value is manually adjusted to best separate the markers from the background. From here we have a binary image which we can work with. Next we apply a simple area filter to remove aberrations which are small in pixel area. The remaining objects are further processed using a erosion and dilation, eccentricity as well as watershed segmentation. Erosion and dilation helps to remove thin dark lines which could be like shadows that are picked up. There are multiple cases where we have seen the markers come into contact with each other when the enter the region of crack propagation. Here to separate the markers we use water shed segmentation. The eccentricity filter is a final filter that only takes objects that are of a minimum eccentricity. We assume that the markers all have a certain level of circularity. These pre processing parameters are set based on an image during the middle of the test. It is good practice to take an image which is difficult to process

as that is likely to be the bottle neck during stretch measurement.

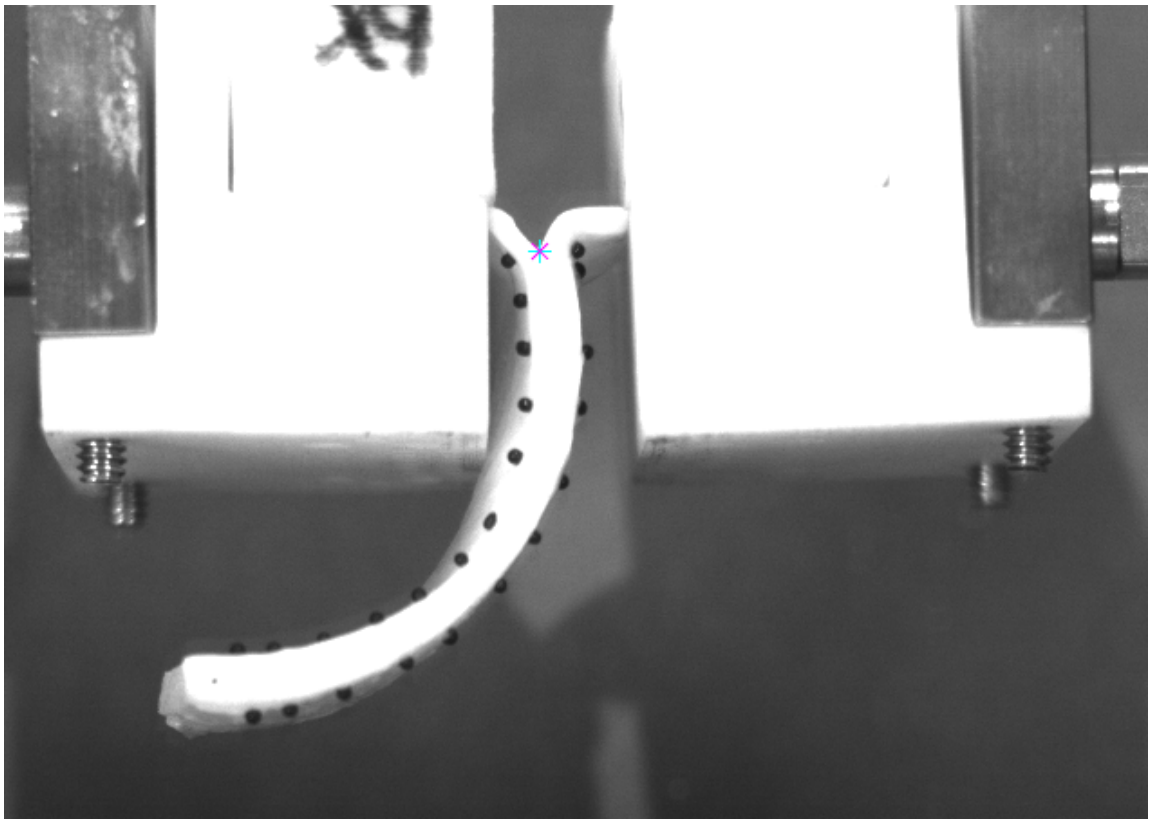

Figure 2.7: Exclusion Frame 1

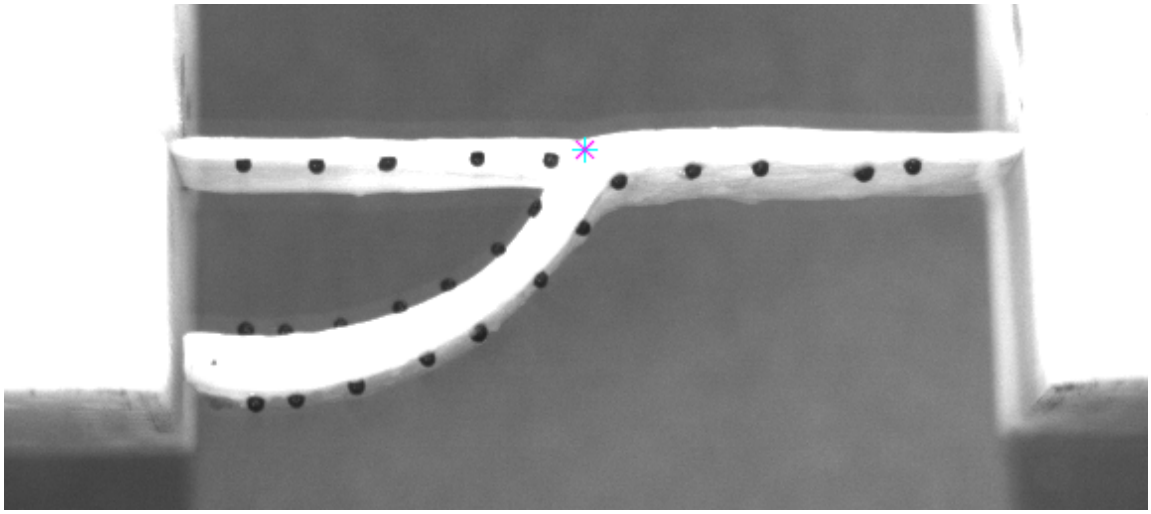

Figure 2.8: Exclusion Frame 300

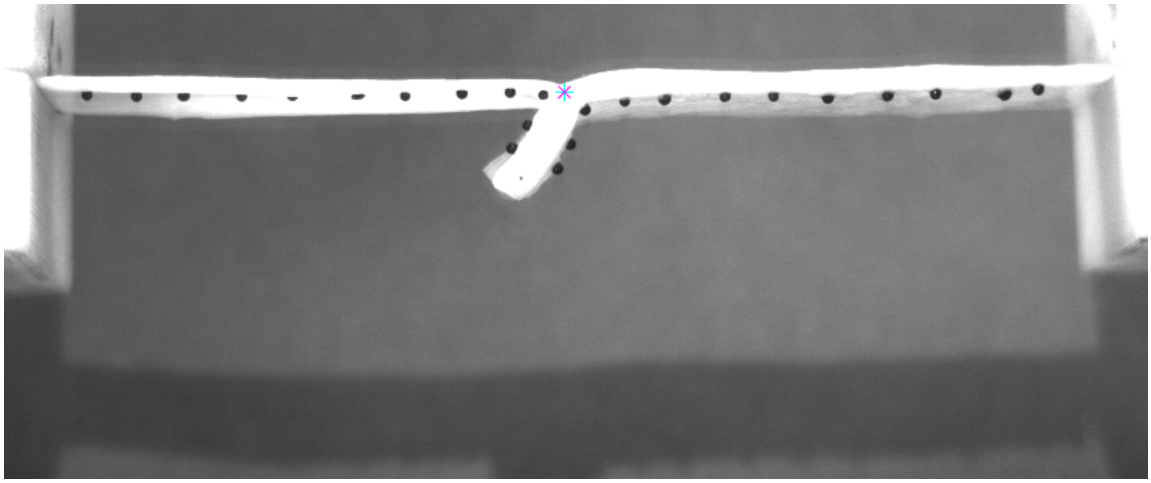

Figure 2.9: Exclusion Frame 700

The markers were decided to be tracked only once they left the region of peeling. So an exclusion region of fixed dimensions was selected for each image. Markers were only tracked and detected if they were outside the exclusion region. Its width was

decided such that the stretch measured would just have reached a constant value. As the crack propagation zone moves throughout the test as the arms are unequally stretched, the position is interpolated between three points taken with equal time gaps throughout the test as can be seen in 2.7, 2.8 and 2.9. The width of the exclusion region was chosen by testing on multiple specimens.

2.2.1.5 Peel Images: Tracking Markers

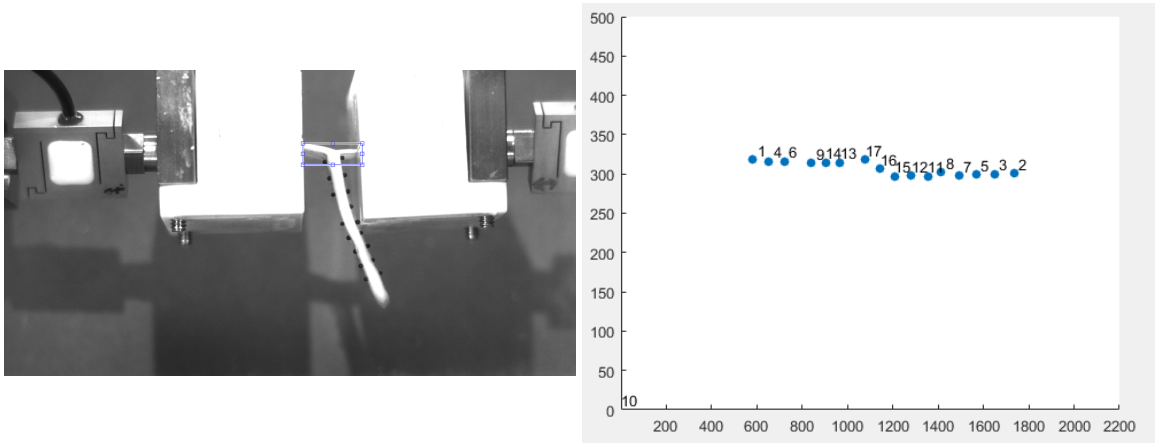

Figure 2.10: (a) Initial Region of Interest (b) Markers Identified Individually

Each image is preprocessed to identify the markers. Their centroids are recorded. After obtaining centroids of markers from all images of the test, they are then linked together. The criterion for linking markers between consecutive frames is decided that: the closest detected marker from the previous frame is the same marker. This assumption need not always hold true but in our situation with a controlled deformation being applied it was sufficient. Otherwise other tracking techniques like velocity must be employed but it was found to be unnecessary in this case.

Handling a new marker entering the region of interest As we attempt to link

the markers from a current frame to the markers from the previous frame we must measure the euclidean distance from a current marker to each detected marker in the previous frame. If the minimum distance is greater than a certain threshold value then it is assumed that this current marker did not appear in the previous frame and so it must be a new marker. It has just exited the region of exclusion and entered the region of interest. This value a search radius was determined by experimenting with various values for different specimen.

Various measures had to be employed to handle issues that arose. It was possible for a marker that was detected well for 200 frames to suddenly not be detected for the next frame. This could be due to varying lighting conditions or even being covered by a portion of the tissue. In this situation the last known position of the marker was recorded in the hope that it would be detected again. Of course this implies that if the marker is not detected for a prolonged period than it will leave the search radius and no longer be linked. Another filter that was used to check the number of frames that a marker was detected compared the total frames from the test. If the ratio was found to be less than 80% then it was assumed to be a distortion that was accidentally picked up.

2.2.1.6 Measuring Stretch

The stretch of a span between two markers was taken as the ratio of their distance in the current frame to their initial distance as measured in the first frame before beginning the test. Spans were taken as the region between two consecutive markers.

2.2.1.7 Issues with Peel

Most of the steps in processing and linking were robust to variations throughout the experiments. Unfortunately there were a few experiments and situations where there was much that could be done to handle the issue.

In particular this ocurred when the sample arms became very thin during testing. The arm displayed a tendency to curl up and no longer remain flat. In this curled state, the markers were covered up by tissue as can be seen in 2.11. The markers were difficult to detect by the naked eye. The processing steps faced difficulty identifying the markers covered by tissue as can be seen in 2.12.

For these specimens incomplete stretch data was obtained.

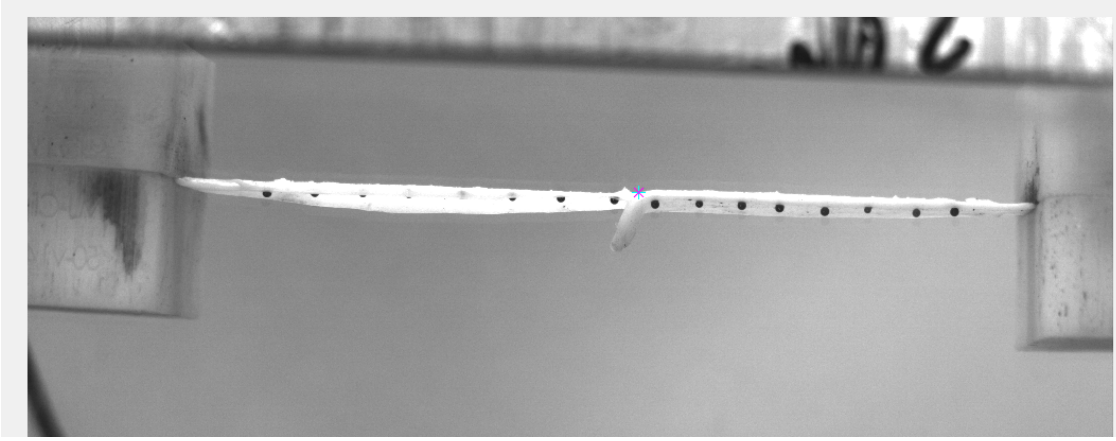

Figure 2.11: Specimen Curling Up

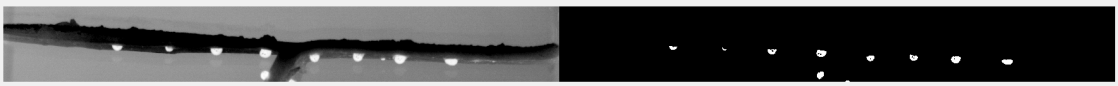

Figure 2.12: Difficulty Identifying Markers

2.2.2 Uniaxial

For the uniaxial tests it was decided to measure deformation using microspheres laid out in a grid pattern. Microspheres have many advantages when compared to

more conventional techniquies like DIC. DIC can be difficult for biological specimens as they must be hydrated. As such applying a speckle pattern can prove to be problematic.

2.2.2.1 Specimen Preparation

On the day of experiments, frozen specimens which are stored at -20 C are thawed over a period of 12 hours at 0 C. Loose connective tissue is carefully removed without damaging the aortic layers. The aorta is cut and layed flat. Along with the peel specimens, rectangular uniaxial specimens are cut out from the different regions. All specimens are tested within 4hrs of thawing.

Microspheres are carefully applied carefully in a grid pattern of 5x5 or 4x4 on the intimal face. Microspheres are touched to adhesive and carefully applied to specimen surfaces. Equal number on either side. With equal spacing as can be seen in 2.13. Microspheres are placed with enough distance between them that they do not come into contact during the uniaxial protocol.

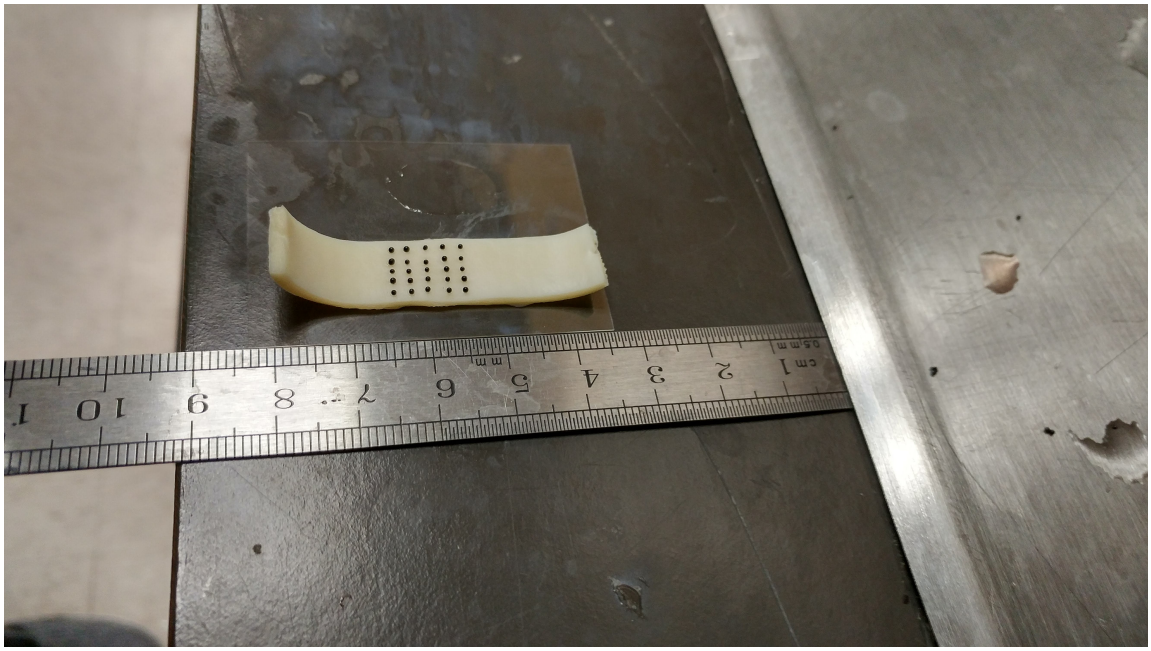

Figure 2.13: Uniaxial Sample

2.2.2.2 Uniaxial Images:Pre-processing

We choose an intial region of interest as can be seen in 2.14a. The height remains constant throughout the test. The width of the region of interest continues to increase according to the rate of movement of the gripping arms.

The image must be processed with many of the same filters as discussed for peel experiments. In this case the images were found to be much less prone to errors and unwanted noise. After preprocessing the centroids from each marker are obtained as can be seen in 2.14b

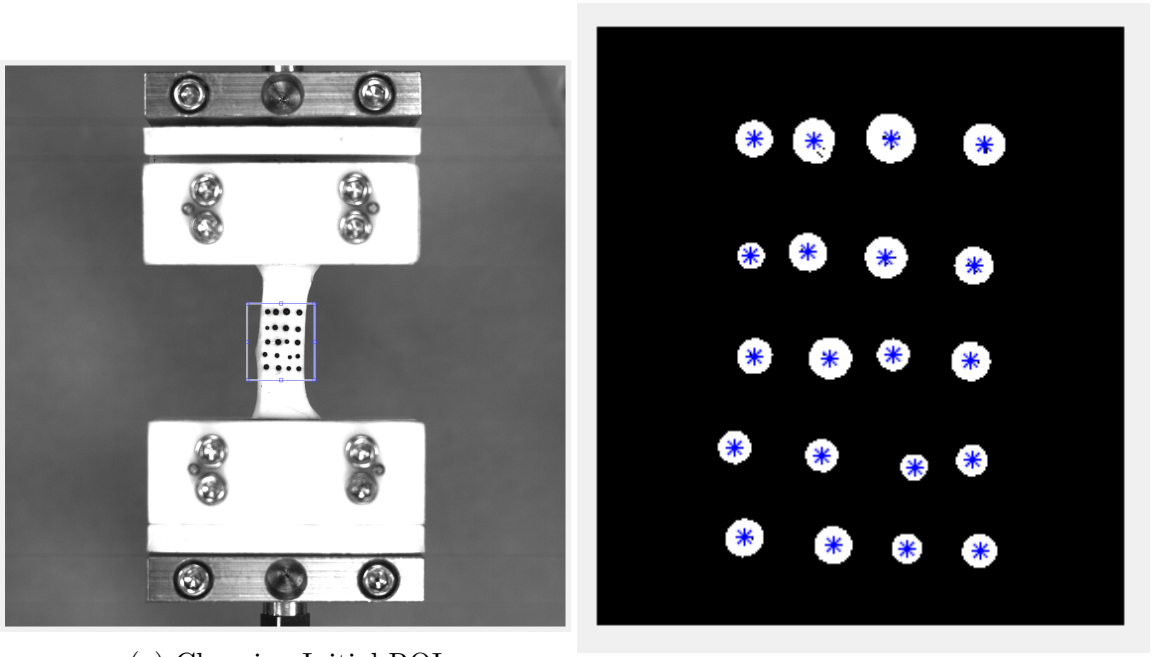

(a) Choosing Initial ROI

(b) Extracting Centroids from Markers for Uniaxial Testing

Figure 2.14: Processing of uniaxial test images

2.2.2.3 Uniaxial Images:Tracking and Obtaining Deformation Quadrilaterals

For tracking and linking markers between frames the same techniques discussed for peel experiments are employed here. The process is simpler in fact as there is no exclusion region and we don't have to worry about markers entering and leaving the region of interest. All markers remain within the region of interest througout the test. The height of the region of interest is increased at the same rate as the peel arms are extending. This ensures that all markers remain inside the peel region.

For obtaining the deformation the grid was broken up into quadrilaterals. Each of the 4 markers for each quadrilateral were ordered in a clockwise order so that the deformation could be obtained and interpolated within the region.

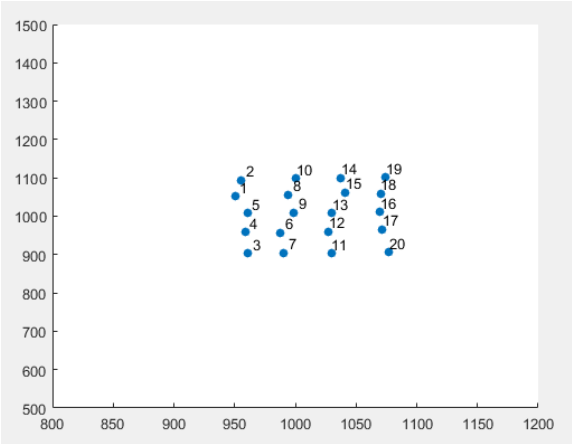

(a) Numbered markers in random order

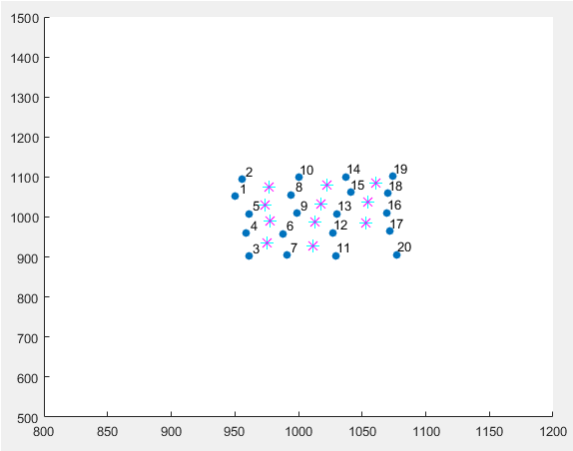

(b) Centroids being ordered into quadrilaterals

Figure 2.15: Obtaining Quadrilaterials for Deformation Calculation Uniaxial Testing

2.2.3 Specimen Dimensions

Specimen dimensions were measured by optical measurement techniques similar to those applied for peeling and uniaxial protocols. For specimen thickness the average thickness was measured between each consecutive set of markers, ie; each span.

The thresholding value was chosen as to separate the specimen from the background as can be seen in 2.16. The background was chosen to have a gray scale value somewhere between that of the markers and that of the specimen. This allows the markers to be identified as well as the contours of the specimen. See 2.17

Figure 2.16: Thresholding Specimen

Figure 2.17: Sample Dimensions

2.3 Results

The stretch for the spans are measured from the moment that they enter the region of interest. In the following plots for stretch, on the X axis is the image number since the start of the experiment. The stretch is only recorded once at least one span has entered the region of interest in each of the intimal and adventitial arms. Stretch is measured to failure in some shorter samples while for longer samples failure was not reached during the peel experiment.

2.19

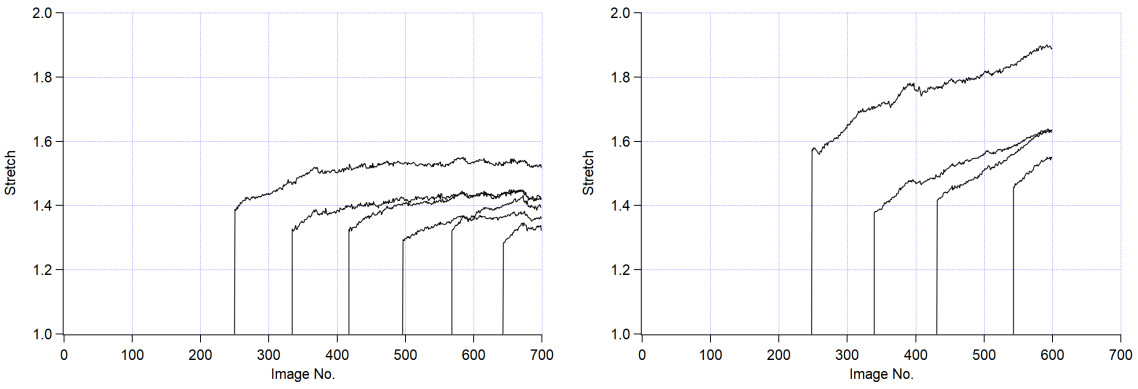

(a) Ascending Circumferential Adventitial (b) Ascending Longitudinal Adventitial

Figure 2.18: Constant and Increasing Stretch

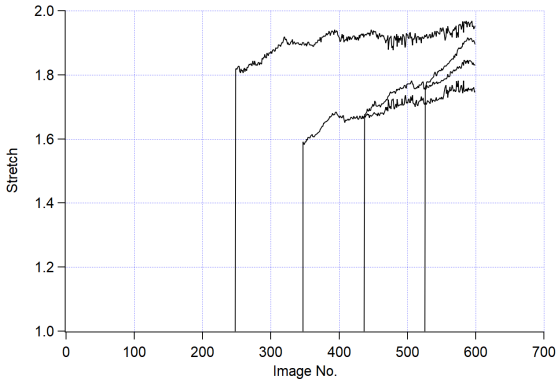

(a) Ascending Longitudinal Intimal

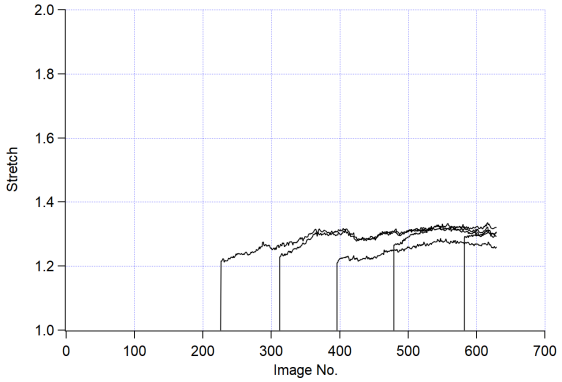

(b) Upper Descending Circumferential Adventitial

Figure 2.19: Variation in Stretch Along Arm

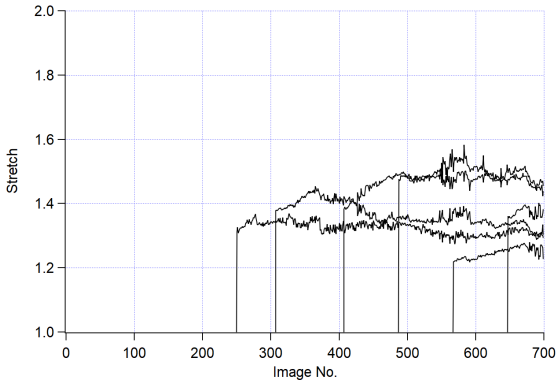

(a) Ascending Circumferential Intimal

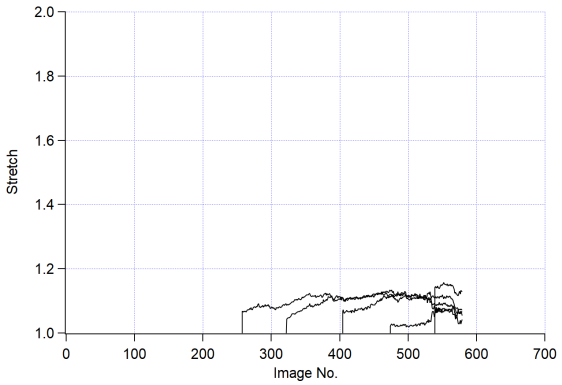

(b) Lower Descending Circumferential Intimal

Figure 2.20: Regional Variations in Stretch

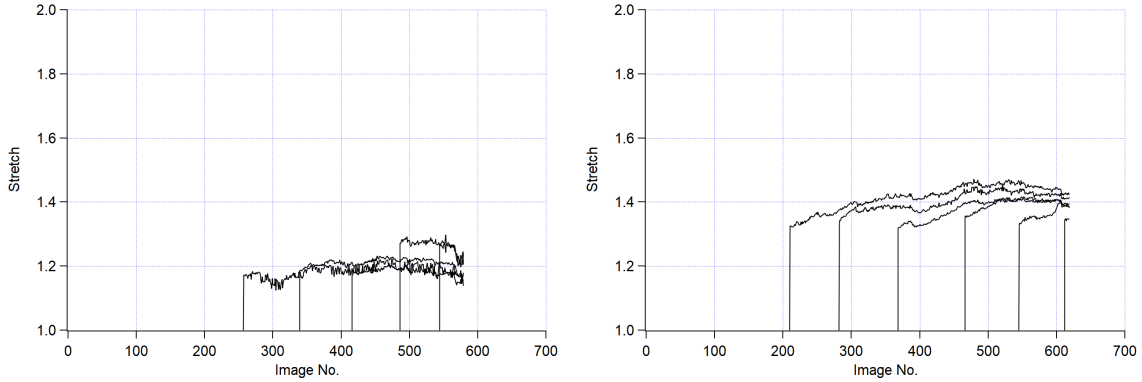

(a) Lower Descending Circumferential Adventitial

(b) Lower Descending Longitudinal Adventitial

Figure 2.21: Directional Variations in Stretch

3. CONCLUSION

From the results we can see that there are significant directional variations in the stretch in figure 2.21. The longitudinal stretch being larger than circumferential stretch across regions and for both intimal and adventitial arms. Earlier observations into the anisotropic nature of the peeling response were made by Sommer et. al [32] The results here indicated higher resisting force/width for axial peeling tests compared to the circumferential peeling tests which was claimed to be proof of anisotropic nature.

The anisotropic property of the aorta was confirmed by Tong et.al [38] in their studies of carotid arteries. 31 pairs of human carotid arteries, both both healthy as well as diseased (atherosclerotic) were tested. The force/width values to separate individual layers were smaller for the circumferential direction compared to the axial direction. Dissection energies per reference area generated during the peeling tests were also lower for the strips in the circumferential direction compared to the axial direction and varied with location. This variation with direction and location is in agreement with the results presented here.

This is further confirmed by [24] Pasta et al. in their studies of aneurysmal and non-aneurysmal ascending thoracic aortas in humans with bicuspid aortic valve as well as tricuspid aortic valve morphology by delamination testing. The force normalized by width, mean value of peeling tension and the peak value of stress indicated a large difference in delamination strength between longitudinal and circumferential directions. Ultimate tensile strength was also greater for circumferential than longitudinal and intimal half was weaker than adventitial half.

Measurement of stretch along the arms of the peel specimens have provided more

insights into the nature of peeling. It can be seen that there are significant regional variations in stretch values in figure 2.20. We see that the ascending aorta yields much higher stretch in the range 1.8-2.0 while lower descending and upper descending have stretch values in the range 1-1.4.

It is seen that the stretch within an arm of the peeling sample can have widely varying stretch values at the end of the experiment as can be seen in figure 2.19. This could be partially attributed to the nature of tear propagation. The tear need not proceed perfectly between two medial layers, between the lamellae. Instead it is possible that the tear can move between layers and this will create a varying thickness and so a variation in stretch. In addition it is important to note that the aorta itself is not of a constant thickness along the length of a sample.

Lastly it is noted that stretch varies with time as well as seen in figure 2.18. In some samples we see that the stretch initially increases and nearly reaches a constant. In other cases it is seen that the stretch increases continuously throughout the experiment, never reaching a constant value.

Future studies could look into the contribution of the various components of the aortic tissue. [23] Noble et al tested specimens after being treated with the appropriate enzymes. Collagenase, Elastase and glutaraldehyde were used to test the response separately.

The limitations of this study are many. Tests were conducted in an open environment and samples were not hydrated. All samples were not of uniform dimensions owing to the difficulty in obtaining samples from each of the regions. Measurement of stretch itself is prone to some variation due to changing lighting conditions.

4. HIGH AMPLITUDE TORSIONAL SHEAR

4.1 Introduction

Studying the mechanics of aortic tissue is a crucial component in understanding its behavior under healthy as well as diseased conditions. Wall shear stress and circumferential stress have been largely accepted as significant factors in arterial growth and remodeling as a response to changes in flow and pressure. But, experimental studies on aortic tissues have largely focused on uniaxial and biaxial tests which are more suited for investigating circumferential stress. This may be explained by the inherent convenience of gripping tissue and then applying deformations in the uniaxial and biaxial modes. As such, the behavior of aortic tissue under shear has been left relatively unstudied. We propose to study the response of porcine aortic wall tissue under cyclic constant torsional shear strain rate for high amplitude (50%) and at different shear strain rates (4%/s and 40%/s). 3 to 4 12.5 mm diameter samples are obtained from the descending porcine aorta. Initial results clearly indicate a non linear response for the moment as a function of the angle of twist while many popular models predict a linear response for the arterial wall even under large shear strain.

In this study we seek to characterize the nonlinear behavior displayed by porcine aortic tissue subjected to large amplitude shear. Wall shear stress and circumferential stress are significant contributing factors to arterial growth and remodeling. While the mechanics of these aortic wall has been studied at length these studies have focused on uniaxial and biaxial tests. These tests study circumferential stresses and have become a standard test for biological materials. Test on the aorta's response to a shearing load has been largely unexplored.

The aorta can undergo shearing deformation in both physiological and non phys-

iological situations[7]. Injury from physical impact like can cause large shear deformation. In addition normal functioning of the aortas can cause shearing. The pulsatile flow of the blood especially at regions of branching of capillaries. This is in addition to shearing caused by hemodynamic shear stress from blood flow on the arterial wall.

In addition, pathological conditions can promote local shearing. Atherosclerosis and calcification can lead to hardening of regions of the wall creating interfaces which may be susceptible. Even due to medical intervention,ie, arterial grafts, or angioplasty wall shearing may occur. As such understanding the effects of these procedures could help us better predict arterial wall remodeling.

Obtaining moment-torsional shear strain information about the arterial walls could help develop complete constitutive models. Current models are good at modeling unaxial and biaxial responses but may not translate well to shear deformations.

Here we aim to lay the ground work for future torsional shear testing using a rheometer on the porcine arterial wall. Contrary to the popular function of a rheometer in this work we are not attempting to study the viscoelastic response, which we are currently investigating. In addition tests have been conducted on the porcine wall as a precursor to possible testing on human tissue due to their anatomical similarities. As such we are investigating the response to some simple but fundamental tests. The first being constant shear rate tests at different amplitudes varying across the possible shear deformations which could be found in the body-from 10% shear strain upto 50% shear strain. In addition we are applying two shear rates at 4%/s and 40%/s for both the lower and upper descending aorta.

Earlier studies on shear of aortas have largely focused on inflation deflation and torsion by twisting [39], [20] and [17]. While more recent studies have used shear testing devices capable of producing shear simultaneously in two orthogonal direc-

tions and measuring the forces in three axes. Human adipose tissue [31] Shear was applied sinusoidally in orthogonal directions for all six modes of shear. Studies have been conducted to understand human myocardium specimen [34],rat myocardium [8] and pig myocardium [9] using a triaxial tester. [2] presented a general approach to study the mechanical behavior of soft materials by applying tensile, compressive or shear loads on a cuboidal myocardium specimen.

Sacks [28] presents a review of techniques used for characterizing soft tissues. The progress from uniaxial to biaxial and finally triaxial tests is discussed along with the difficulties of integrating the constitutive model with the experimental test.

Horgan et al. [15] review the challenges in conducting simple shear experiments and in obtaining the parameters for constitutive models. Simple shear of fibre reinforced elastic materials, shear response for soft tissues, the effects of fiber orientation, shear stress on inclined faces and normal stress response are discussed along with the past attempts to address these issues.

Shuck et al. [30] characterized the shear response of brain tissue using a torsional rheometer to shed light on the response during head injury impacts. The linear viscoelastic properties are determined using a four-parameter model. Failure criteria are studied based on maximum shear strain and strain rate.

Janmey et al.[18] discuss the reasons why rheology applied to biological materials is a field that should be looked into. There is a basic explanation of rheology principles followed by concerns to consider while designing an experimental setup to study biological tissues. They discuss the special considerations to be considered for biological materials like their frailness, nonlinearity, and the small range of strains possible.

The authors mention the difficulties in studying biological tissues like how tissues undergo biochemical changes after isolation and storing. Another major issue is

the heterogeneity of tissues. They are multilayered, consisting of many cell types each with its own mechanical properties, orientation, and strength. Although it is mentioned that there are materials in use today that exhibit similar levels of complexity like carbon fiber composites.

4.2 Methods

4.2.1 Specimen Harvest

Heart and aorta are collected from freshly killed hogs from a slaughterhouse on Texas A&M University campus. Samples are placed in an ice box for transportation to the lab. Using dissection tools, the aorta is separated from the heart and is cut into thoracic and abdominal segments. The thoracic aorta is further divided into upper descending and lower descending regions. These samples are stored at -20^{0}C in centrifuge tubes containing Phosphate buffer saline(PBS) solution.

4.2.2 Specimen Preparation

On the day of experiments, frozen specimens which are stored at -20 C are thawed over a period of 12 hours at 0 C. Loose connective tissue is carefully removed without damaging the aortic layers. The aorta is cut and layed flat. Specimens of 12.5 mm diameter are punched out from the tissue. Around 4 samples per segment in both descending and ascending aorta are obtained.The specimens are stored in PBS at 0 C until the time of testing. All specimens are tested within 4hrs of thawing.

As much as possible, connective tissue is removed by teasing and cutting. The sample to be tested is taken out and dried with soft tissues.

4.2.3 Experiment Protocol

Next the specimen is attached to the rheometer plates. Cyanoacrylate adhesive is applied on the upper stainless steel attachment surface. The specimens adventitial

side is held pressed against upper surface surface for 30 s to adhere. Next adhesive is applied on the lower surface and the sample is held at 1N for 5 min for complete adherence. This allows for the bond to form that's strong enough such that there won't be attachment during the test.

Next, the specimen is attached to the rheometer plates. A cyanoacrylate adhesive is applied to the upper stainless steel attachment surface. The specimen thickness is measured between two parallel plates under less than .15 N normal load. Before beginning the test PBS solution is added to create a bath at 25 Celsius.

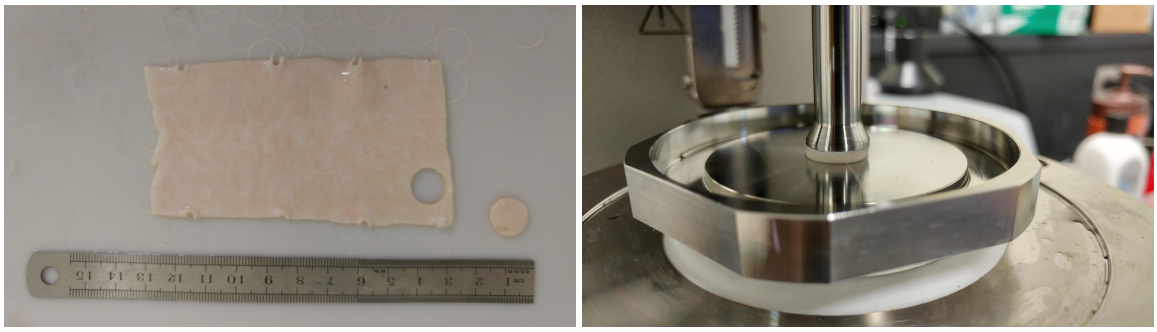

Figure 4.1: (a) Aorta cut open and spread out with specimen punch holes (b) Specimen on rheometer before introducing water bath

The test is started with 50% shear strain amplitude cyclic at a constant shear rate. 10 cycles at 50,40,30,20 and 10% shear strain amplitude are completed for each sample at two different shear rates. The two rates are 4% shear per second and 40% shear strain per second. The total test duration is 28 minutes for each specimen. Around 3-4 samples per segment are tested, both from the upper and lower thoracic aorta.

4.3 Results

Results from a representative shear test in which cyclic constant shear rate of 4%/s at shear strains between 10% and 50% can be seen in **??** In 4.4 there are results from samples obtained from each of the upper and lower descending aorta regions. The final cycles from each amplitude of applied shear strains can be seen here.

In **??** again we have moment-shear strain plots from the final cycle of the 50% shear strain amplitude response. Included in the plots are both the 4% as well as 40% shear strain/s responses for samples obtained from the upper and descending aorta.

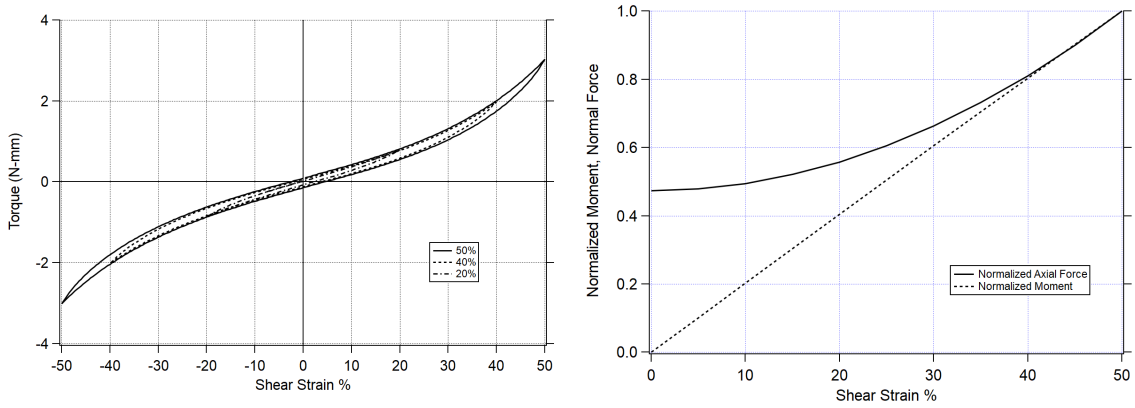

Figure 4.2: Overlap of Response and Nonlinear Behavior

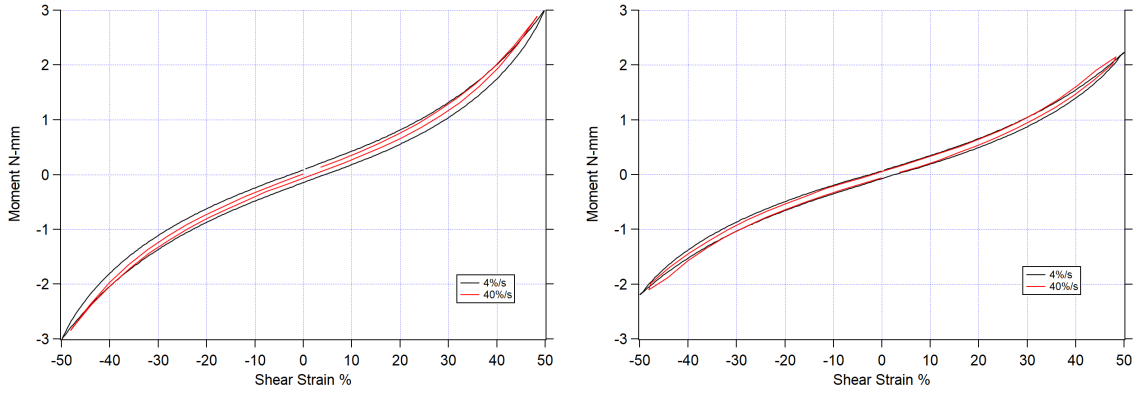

Figure 4.3: Rate Dependence

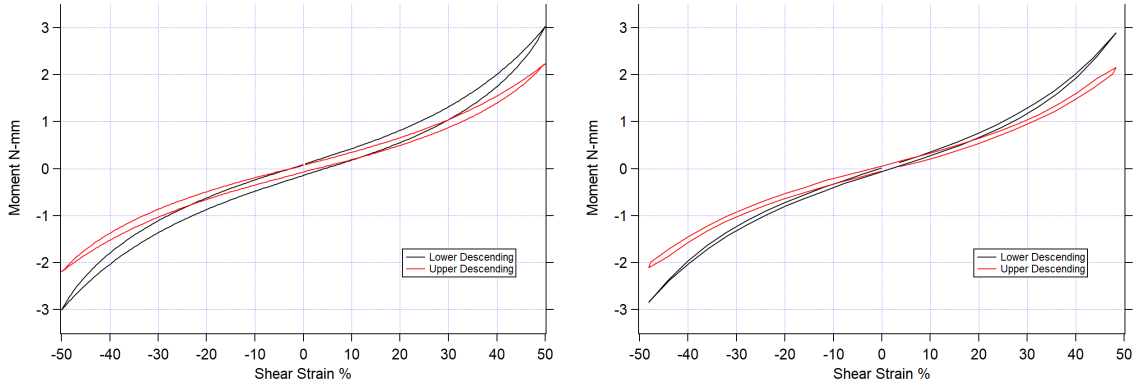

Figure 4.4: Regional Variation

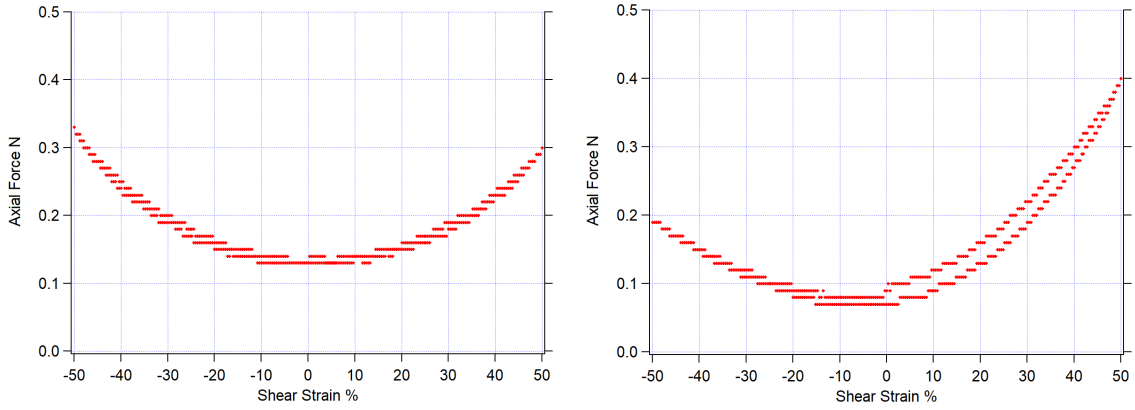

Figure 4.5: Normal Force

Aorta	Sample	Normal Force (N)	Thickness (mm)
17	a	0.16	1.711
17	b	0.13	2.569
17	c	0.15	1.669
17	d	0.15	2.698
23	a	0.15	1.824
23	b	0.16	1.757
23	c	0.12	1.683
23	d	0.14	1.851
22	a	0.05	1.585
22	b	0.22	1.651
22	c	0.15	1.550
21	a	0.21	2.206
21	b	0.21	2.048
21	c	0.14	2.385
21	d	0.15	1.913

Table 4.1: Lower Descending Aorta Dimensions

Aorta	Sample	Normal Force (N)	Thickness (mm)
17	a	0.16	1.260
17	b	0.16	1.385
17	c	0.14	1.456
23	a	0.16	1.621
23	b	0.15	1.430
23	c	0.15	1.312
23	d	0.16	1.582
22	a	0.23	1.282
22	b	0.08	1.160
22	c	0.15	1.358
22	d	0.15	1.395
21	a	0.15	1.373
21	b	0.13	1.203
21	c	0.08	1.278
21	d	0.17	1.084

Table 4.2: Upper Descending Aorta Dimensions

5. CONCLUSION

From the response, it can be seen that the initial nearly linear response becomes nonlinear at around 20% shear strain **??**. In one of the only other studies on shear on the aorta wall, [11] translational shearing tests were conducted on bovine aortas and a linear relationship was found between shear strain and shear stress. Translational stretch of upto 1.6 was applied on specimens of 6mm by 6mm dimensions in both the circumferential and longitudinal directions. No difference was found between shearing in circumferential and longitudinal directions. Additionally the effect of compression on the response was studied. There were significant variations in the shear response between samples. In [17] the shear modulus of the bovine aorta was measured. Rectangular strips of the aorta wall were taken and clamped at the two ends and a shear deformation was applied via a central guideline. Shear was measured by observing change in position of four markers placed in a square pattern. A linear relationship between shear stress and shear strain was observed here. In addition it is important to note that one of the most popular models, the Holzapfel-Osser-Ogden model, estimates a linear response; Fig. 4.2. Parameters for abdominal aorta are used from [**?**].

We see a clear variation between the response for the upper and lower descending samples as can be seen in 2.20. The magnitude of the moment is much larger for the lower descending aorta.

The small effect of variation of strain rate as can be seen in 4.3 is in agreement with previous experiments. Arterial tissue is accepted to behave repeatably after cyclic loading and preconditioning. The response does not change with a variation of the strain rate.

The results from our tests demonstrate a remarkable level of repeatability in the responses across specimens that is rarely seen in tests on biological tissues. A few characteristic traits of the moment-shear strain curves were common across the samples. The response was found to be almost identical under both positive and negative shear strain. The torque range was between 2 and 6 N-mm. Additionally, the torque-shear strain loops are overlapping **??** for the different shear amplitudes. This was not observed by [8] while testing porcine myocardium under shearing.

The normal force-shear strain response curves appear to be skewed in contrast to the torque-shear strain as can be seen in 4.5. Very few samples gave similar normal force responses for both positive and negative shear strain displacements.

Other studies on shear of aortic tissue have used a triaxial torsion machine; [20] observed a linear relationship between twist angle and torque in the range of inflations and longitudinal extensions for porcine coronary aorta. No difference was reported between the direction of twist. [35] tested dissected aorta wall under shear in 6 different shear modes to better understand rupture properties for Aortic Dissection.

It is accepted that collagen fibers are the load bearing members at large deformations. In [35] it is suggested that the elastin network, consisting of elastic lamellae, elastin fibers, and radial elastin fibers have little influence in arterial shear strength at higher deformations. In many models collagen fibers are considered to be oriented parallel to the plane of shearing and so would have little effect. It is noted that these collagen fibers are interconnected by smooth muscle cells, and an elastin network and so it is not very clear as to the load bearing members under shear loads.

It is important to note the limitations of this study. The samples were assumed to be of uniform thickness. This was the reason we used half inch specimens. The surfaces of the sample are assumed to be completely adhered to the plates of the rheometer. In reality there could have been patches of adherence. We assume that

the properties do not change throughout the test due to loss of hydration or exposure to the environment. The samples were all frozen at -20 C before thawing and testing. This freezing and thawing cycle has unknown effects although (). The adhesive was assumed not to diffuse too deeply into the tissue, although some diffusion is required for adhesion.

REFERENCES

[1] Adam C Abraham, Christian R Edwards, Gregory M Odegard, and Tammy L Haut Donahue. Regional and fiber orientation dependent shear properties and anisotropy of bovine meniscus. *Journal of the Mechanical Behavior of Biomedical Materials*, 4:2024–2030, 2011.

[2] Reza Avazmohammadi, David S. Li, Thomas Leahy, Elizabeth Shih, João S. Soares, Joseph H. Gorman, Robert C. Gorman, and Michael S. Sacks. An integrated inverse model-experimental approach to determine soft tissue three-dimensional constitutive parameters: application to post-infarcted myocardium. *Biomechanics and Modeling in Mechanobiology*, 17(1):31–53, feb 2018.

[3] Mehmet Ayyildiz, Soner Cinoglu, and Cagatay Basdogan. Effect of normal compression on the shear modulus of soft tissue in rheological measurements. *Journal of the Mechanical Behavior of Biomedical Materials*, 49:235–243, sep 2015.

[4] Takehiko AZUMA and Masamitsu HASEGAWA. A RHEOLOGICAL APPROACH TO THE ARCHTECTURE OF ARTERIAL WALLS. *The Japanese Journal of Physiology*, 21(1):27–47, 1971.

[5] Anju R. Babu, Achu G. Byju, and Namrata Gundiah. Biomechanical Properties of Human Ascending Thoracic Aortic Dissections. *Journal of Biomechanical Engineering*, 137(8):081013, aug 2015.

[6] Micheal Carson and Margot Roach. Carson MW, Roach MR. The strength of the aortic media and its role in the propagation of aortic dissection. *J Biomechanics*, 23, 1990.

[7] S X Deng, J Tomioka, J C Debes, and Y C Fung. New experiments on shear modulus of elasticity of arteries. *J. Physiol.Heart Circ. Physiol*, 266(35), 1994.

[8] Socrates Dokos, Ian J. LeGrice, Bruce H. Smaill, Julia Kar, and Alistair A. Young. A Triaxial-Measurement Shear-Test Device for Soft Biological Tissues. *Journal of Biomechanical Engineering*, 122(5):471, oct 2000.

[9] Socrates Dokos, Bruce H Smaill, Alistair A Young, and Ian J LeGrice. Shear properties of passive ventricular myocardium. *American Journal of Physiology-Heart and Circulatory Physiology*, 283(6):H2650–H2659, 2002.

[10] B S Gow and M G Taylor. Measurement of viscoelastic properties of arteries in the living dog. *Circulation research*, 23(1):111–22, jul 1968.

[11] Henry W. Haslach, Lauren N. Leahy, Parinaz Fathi, Joshua M. Barrett, Amanda E. Heyes, Thomas A. Dumsha, and Eileen L. McMahon. Crack Propagation and Its Shear Mechanisms in the Bovine Descending Aorta. *Cardiovascular Engineering and Technology*, 6(4):501–518, dec 2015.

[12] A E HIRST and V J JOHNS. Experimental dissection of media of aorta by pressure. Its relation to spontaneous dissecting aneurysm. *Circulation research*, 10(6):897–903, jun 1962.

[13] G.A. Holzapfel, T.C. Gasser, and M. Stadler. A structural model for the viscoelastic behavior of arterial walls: Continuum formulation and finite element analysis. *European Journal of Mechanics - A/Solids*, 21(3):441–463, jan 2002.

[14] Gerhard A. Holzapfel. Structural and Numerical Models for the (Visco)elastic Response of Arterial Walls with Residual Stresses. In *Biomechanics of Soft Tissue in Cardiovascular Systems*, pages 109–184. Springer Vienna, Vienna, 2003.

[15] Cornelius O Horgan and Jeremiah G Murphy. Simple shearing of soft biological tissues. *Proc. R. Soc. A*, 467:760–777, 2011.

[16] T Imura, K Yamamoto, T Satoh, K Kanamori, T Mikami, and H Yasuda. In vivo viscoelastic behavior in the human aorta. *Circulation research*, 66(5):1413–9, may 1990.

[17] A Tozeren J. Vossoughi. DETERMINATION OF AN EFFECTIVE SHEAR MODULUS OF AORTA. *Russian Journal of Biomechanics*, pages 20–35, 1998.

[18] Paul A. Janmey, Penelope C. Georges, and Søren Hvidt. Basic Rheology for Biologists. *Methods in Cell Biology*, 83:1–27, jan 2007.

[19] B M Learoyd and M G Taylor. Alterations with age in the viscoelastic properties of human arterial walls. *Circulation research*, 18(3):278–92, mar 1966.

[20] X. Lu, J. Yang, J. B. Zhao, H. Gregersen, and G. S. Kassab. Shear modulus of porcine coronary artery: contributions of media and adventitia. *American Journal of Physiology-Heart and Circulatory Physiology*, 285(5):H1966–H1975, nov 2003.

[21] N. F. MacLean, N. L. Dudek, and M. R. Roach. The role of radial elastic properties in the development of aortic dissections. *Journal of Vascular Surgery*, 1999.

[22] Amir K Miri, Rosaire Mongrain, Lei Xi Chen, and Luc Mongeau. Quantitative assessment of the anisotropy of vocal fold tissue using shear rheometry and traction testing. *Journal of biomechanics*, 45(16):2943–6, nov 2012.

[23] Christopher Noble, Nicole Smulders, Roger Lewis, Matt J Carré, Steve E Franklin, Sheila MacNeil, and Zeike A Taylor. Controlled peel testing of a

model tissue for diseased aorta. *Journal of biomechanics*, 49(15):3667–3675, nov 2016.

[24] Salvatore Pasta, Julie A. Phillippi, Thomas G. Gleason, and David A. Vorp. Effect of aneurysm on the mechanical dissection properties of the human ascending thoracic aorta. *The Journal of Thoracic and Cardiovascular Surgery*, 143(2):460–467, feb 2012.

[25] D J Patel, J S Janicki, R N Vaishnav, and J T Young. Dynamic anisotropic viscoelastic properties of the aorta in living dogs. *Circulation research*, 32(1):93–107, jan 1973.

[26] J. S. Robertson and K. Viner Smith. An analysis of certain factors associated with the production of experimental dissection of the aortic media, in relation to the pathogenesis of dissecting aneurysm. *The Journal of Pathology and Bacteriology*, 60(1):43–49, jan 1948.

[27] Anna-Katharina Rohlfs, Eric Goodyer, Till Clauditz, Markus Hess, Malte Kob, Susan Koops, Klaus Püschel, Frank W. Roemer, and Frank Müller. The anisotropic nature of the human vocal fold: an ex vivo study. *European Archives of Oto-Rhino-Laryngology*, 270(6):1885–1895, may 2013.

[28] Michael S Sacks and Wei Sun. MULTIAXIAL MECHANICAL BEHAVIOR OF BIOLOGICAL MATERIALS. *Annu. Rev. Biomed. Eng*, 5:251–84, 2003.

[29] Selda Sherifova. Modeling the Propagation of Aortic Dissection. 2015.

[30] L. Z. Shuck and S. H. Advani. Rheological Response of Human Brain Tissue in Shear. *Journal of Basic Engineering*, 94(4):905, dec 1972.

[31] Gerhard Sommer, Maximilian Eder, Laszlo Kovacs, Heramb Pathak, Lars Bonitz, Christoph Mueller, Peter Regitnig, and Gerhard A. Holzapfel. Multi-

axial mechanical properties and constitutive modeling of human adipose tissue: A basis for preoperative simulations in plastic and reconstructive surgery. *Acta Biomaterialia*, 9(11):9036–9048, nov 2013.

[32] Gerhard Sommer, T. Christian Gasser, Peter Regitnig, Martin Auer, and Gerhard A. Holzapfel. Dissection Properties of the Human Aortic Media: An Experimental Study. *Journal of Biomechanical Engineering*, 130(2):021007, 2008.

[33] Gerhard Sommer, Daniel Ch Haspinger, Michaela Andr, Michael Sacherer, Christian Viertler, Peter Regitnig, and Gerhard A Holzapfel. Quantification of Shear Deformations and Corresponding Stresses in the Biaxially Tested Human Myocardium. *Annals of Biomedical Engineering*.

[34] Gerhard Sommer, Andreas J Schriefl, Michaela Andrä, Michael Sacherer, Christian Viertler, Heimo Wolinski, and Gerhard A Holzapfel. Biomechanical properties and microstructure of human ventricular myocardium. *Acta Biomaterialia*, 24:172–192, 2015.

[35] Gerhard Sommer, Selda Sherifova, Peter J Oberwalder, Otto E Dapunt, Patricia A Ursomanno, Abe Deanda, Boyce E Griffith, and Gerhard A Holzapfel. Mechanical strength of aneurysmatic and dissected human thoracic aortas at different shear loading modes. 2016.

[36] A S Tam, M C Sapp, and M R Roach. The effect of tear depth on the propagation of aortic dissections in isolated porcine thoracic aorta. *Journal of biomechanics*, 31(7):673–6, jul 1998.

[37] I. M. Tiessen and M. R. Roach. Factors in the Initiation and Propagation of Aortic Dissections in Human Autopsy Aortas. *Journal of Biomechanical Engineering*, 115(1):123, feb 1993.

[38] Jianhua Tong, Gerhard Sommer, Peter Regitnig, and Gerhard A. Holzapfel. Dissection Properties and Mechanical Strength of Tissue Components in Human Carotid Bifurcations. *Annals of Biomedical Engineering*, 39(6):1703–1719, jun 2011.

[39] E.E Tseders V.A. Kasyanov, B.A. Purinya. Determination of the Shear Modulus of Human Blood Vessel Walls. *Polymer Mechanics*, (2), 1979.

[40] C van Baardwijk and M R Roach. Factors in the propagation of aortic dissections in canine thoracic aortas. *Journal of biomechanics*, 20(1):67–73, jan 1987.

[41] Norman Y. Yao, Ryan J. Larsen, and David A. Weitz. Probing nonlinear rheology with inertio-elastic oscillations. *Journal of Rheology*, 52(4):1013–1025, jul 2008.

[42] John T. Young, Ramesh N. Vaishnav, and Dali J. Patel. Nonlinear anisotropic viscoelastic properties of canine arterial segments. *Journal of Biomechanics*, 10(9):549–559, jan 1977.

[43] Tosh ! Yuj, T Tanaka, and Yuan-Cheng Fungi. ELASTIC AND INELASTIC PROPERTIES OF THE CANINE AORTA AND THEIR VARIATION ALONG THE AORTIC TREE*.

[44] Wei Zhang, Yi Liu, and Ghassan S. Kassab. Viscoelasticity reduces the dynamic stresses and strains in the vessel wall: implications for vessel fatigue. *American Journal of Physiology-Heart and Circulatory Physiology*, 293(4):H2355–H2360, oct 2007.

[45] Yu Zou and Yanhang Zhang. The orthotropic viscoelastic behavior of aortic elastin. *Biomechanics and Modeling in Mechanobiology*, 10(5):613–625, oct 2011.

APPENDIX A

STRETCH MEASUREMENT

In the following pages is the custom code for peel stretch measurement.

Table of Contents

Initialize

```
close all;
clearvars -except indist_l indist_r;
clc;
clear figs;
recordflag=0;
```

Load initial distances

```
indis=load('indist.mat');
indist_l=indis.indist_l;
indist_r=indis.indist_r;
```

```
Error using load
Unable to read file 'indist.mat'. No such file or directory.

Error in stretch (line 8)
indis=load('indist.mat');
```

Read in image

```
specimen='BMEL-18-09-020-F ';
imagename='Vimba_0_';
filextbmp='.bmp';
im_i=input('Which image would you like to use for parameters?
 \n','s');
fnamebmp=strcat(imagename,im_i,filextbmp);
A=imread(fnamebmp);
B=A;
```

Crop Region of Interest

```
disp('Crop region of interest \n');
[C,C_rect]=imcrop(B);
close
```

Crop Region to be Excluded from ROI

```
w_exc=150
h_exc=150

exc_frame1=input('Which image would you like to use for exclusion box
 1? \n','s');
fnamebmp=strcat(imagename,exc_frame1,filextbmp);
exc_frame1=str2num(exc_frame1);
im_exc1=imread(fnamebmp);

imshow(im_exc1)
disp('Choose center of crack propogation region \n');
[x,y] = getpts
close;
Xmin_exc1=x-w_exc/2
Xmax_exc1=x+w_exc/2
Ymin_exc1=y+h_exc/2


exc_frame2=input('Which image would you like to use for exclusion box
 2? \n','s');
```

```
fnamebmp=strcat(imagename,exc_frame2,filextbmp);
im_exc2=imread(fnamebmp);
exc_frame2=str2num(exc_frame2);

imshow(im_exc2)
disp('Choose center of crack propogation region \n');
[x,y] = getpts
close;
Xmin_exc2=x-w_exc/2
Xmax_exc2=x+w_exc/2
Ymin_exc2=y+h_exc/2


exc_frame3=input('Which image would you like to use for exclusion box
 3? \n','s');
fnamebmp=strcat(imagename,exc_frame3,filextbmp);
im_exc3=imread(fnamebmp);
exc_frame3=str2num(exc_frame3);

imshow(im_exc3)
disp('Choose center of crack propogation region \n');
[x,y] = getpts
close;
Xmin_exc3=x-w_exc/2
Xmax_exc3=x+w_exc/2
Ymin_exc3=y+h_exc/2
```

First we obtain the markers

Choose threshold such that all markers are visible

```
flag=0;
D=imcomplement(C);
while flag==0
    T=input('Please enter the thresholding value between 0 and 1 to
 locate markers \n');
    E=imbinarize(D,T);
    figure;
    imshowpair(D,E,'montage')
    done=input('Change threshold? y/n \n','s');
    close
    if done=='n';
        flag=1;
    end
end
```

Apply area filter

```
flag=0;
while flag==0
    ar=input('Would you like to use default area filter? y/n \n','s');
    if ar=='y'
        areamax=400;
```

```
        areamin=30;
    elseif ar=='n'
        areamin=input('Enter min area');
        areamax=input('Enter max area');
    end
    areafilterE=bwareafilt(E,[areamin areamax]);
    figure
    title('Area filter ')
    imshowpair(E,areafilterE,'montage');
    done=input('Change area filter? y/n \n','s');
    close
    if done=='n';
        flag=1;
    end
end
```

Erode and dilate

```
flag=0;

while flag==0
    er=input('Would you like to use default erode and dilate values?
 y/n \n','s');
    if er=='y'
        r_er='2';
        r_dil='4';
    elseif er=='n'
        r_er=input('Enter erosion radius y/n \n','s');
        r_dil=input('Enter dilation radius y/n \n','s');
    end
    SE_er = strel('diamond',str2double(r_er));
    SE_dil = strel('diamond',str2double(r_dil));
    IM = imerode(areafilterE,SE_er);
    G = imdilate(IM,SE_dil);
    figure
    imshowpair(areafilterE,G,'montage');
    done=input('Change erosion and dilation? y/n \n','s');
    close
    if done=='n';
        flag=1;
    end
end
```

Compute convex polygon and centroid for each object

```
conveximage = regionprops(G,'ConvexImage');
centroids=regionprops(G,'Centroid');
eccentricity=regionprops(G,'Eccentricity');
solidity=regionprops(G,'Solidity');
cens_temp = cat(1, centroids.Centroid);
```

```
eccs=cat(1,eccentricity.Eccentricity);
sols=cat(1,solidity.Solidity);
```

Filter on solidity

```
flag=0;
while flag==0
    s=input('Would you like to use default solidity filter values? y/n
 \n','s');
    if s=='y'
        soliditymin=.7;
    elseif s=='n'
        soliditymin=input('Enter min solidity');
    end

    j=1;
    for i=1:length(cens_temp)
        if (sols(i)>soliditymin)
            cens_temp2(j,1:2)=cens_temp(i,:);
            j=j+1;
        end
    end
    figure
    imshow(areafilterE)
    hold on
    plot(cens_temp2(:,1),cens_temp2(:,2), 'b*')
    hold off
    done=input('Change solidity filter? y/n \n','s');
    close
    if done=='n';
        flag=1;
    end
end
```

Filter on eccentricity

```
flag=0;
while flag==0
    e=input('Would you like to use default eccentricity filter values?
 y/n \n','s');
    if e=='y'
        eccmax=.9;
    elseif e=='n'
        eccmax=input('Enter max eccentricity');
    end
    j=1;
    for i=1:length(cens_temp2)
        if (eccs(i)<eccmax)
            cens(j,1:2)=cens_temp2(i,:);
            j=j+1;
        end
    end
```

```
    figure
    imshow(areafilterE)
    hold on
    plot(cens(:,1),cens(:,2), 'b*')
    hold off
    done=input('Change eccentricity filter? y/n \n','s');
    close
    if done=='n';
        flag=1;
    end
end
```

To plot superimposed centroids of each object in the image

```
figure
imshow(areafilterE)
hold on
plot(cens(:,1),cens(:,2), 'b*')
hold off
disp('Press key to continue\n');
w = waitforbuttonpress;
close
cens=0;
```

Now measure distance between markers in region of interest during test

Read in image

```
im_in=input('Which image would you like to start measurement from?
 \n','s');
im_fin=input('Which image would you like to end measurement? \n','s');
fnamebmp=strcat(imagename,im_in,filextbmp);
A=imread(fnamebmp);
B=A;
```

Choose inital ROI

Crop Region of Interest

```
disp('Crop region of interest \n');

[in,in_rect]=imcrop(B);

close;

record_i=0;
```

```
recordflag=0;
for im_i=str2num(im_in):str2num(im_fin)
```

Read in image

```
fnamebmp=strcat(imagename,num2str(im_i),filextbmp);
A=imread(fnamebmp);
B=A;
```

Crop Region of Interest

```
Xmin=in_rect(1)-(im_i+1-str2num(im_in))*1;
Ymin=in_rect(2);
w=in_rect(3)+(im_i+1-str2num(im_in))*2;
h=in_rect(4);
B_rect=[Xmin Ymin w h];
C=imcrop(B,B_rect);
```

Exclusion Box

```
if (im_i>exc_frame1 && im_i<=exc_frame2)
    exc_f_ratio=(im_i-exc_frame1)/(exc_frame2-exc_frame1);
    Xmin_exc=(1-exc_f_ratio)*Xmin_exc1+exc_f_ratio*Xmin_exc2;
    Xmax_exc=(1-exc_f_ratio)*Xmax_exc1+exc_f_ratio*Xmax_exc2;

elseif (im_i>exc_frame2 && im_i<=exc_frame3)
    exc_f_ratio=(im_i-exc_frame2)/(exc_frame3-exc_frame2);
    Xmin_exc=(1-exc_f_ratio)*Xmin_exc2+exc_f_ratio*Xmin_exc3;
    Xmax_exc=(1-exc_f_ratio)*Xmax_exc2+exc_f_ratio*Xmax_exc3;
else
    Xmin_exc=Xmin_exc1;
    Xmax_exc=Xmax_exc1;
end
```

First we obtain the markers

Choose threshold such that all markers are visible

```
D=imcomplement(C);
E=imbinarize(D,T);
```

Apply area filter

```
areafilterE=bwareafilt(E,[areamin areamax]);
```

Erode and dilate

```
IM = imerode(areafilterE,SE_er);
G = imdilate(IM,SE_dil);
```

Compute convex polygon and centroid for each object

```
conveximage = regionprops(G,'ConvexImage');
centroids=regionprops(G,'Centroid');
eccentricity=regionprops(G,'Eccentricity');
solidity=regionprops(G,'Solidity');
cens_temp = cat(1, centroids.Centroid);
eccs=cat(1,eccentricity.Eccentricity);
sols=cat(1,solidity.Solidity);
```

Filter on solidity and eccentricity

```
j=1;
[m,n]=size(cens_temp);
for i=1:m
    if (sols(i)>soliditymin && eccs(i)<eccmax)
        cens_temp1(j,1:2)=cens_temp(i,1:2);
        j=j+1;
    end
end
if j==1
    cens=0;
else
```

Adjust X and Y to global values

```
    [m,n]=size(cens_temp1);
    for i=1:m
        cens_temp1(i,1)=cens_temp1(i,1)+Xmin;
        cens_temp1(i,2)=cens_temp1(i,2)+Ymin;
    end
```

Filter out centroids that are outside region of interest

```
    j=1;
    markerflag=0;
    for i=1:m
        if (cens_temp1(i,1)>Xmax_exc || cens_temp1(i,1)<Xmin_exc)
            cens(j,1:2)=cens_temp1(i,1:2);
            j=j+1;
            markerflag=markerflag+1;
        end
    end
    if j==1
        cens=0;
    end
```

to check and troubleshoot

```
%To plot superimposed centroids of each object in the image
%               if markerflag>0
%                  figure
%                  imshow(areafilterE)
%                  hold on
%                  plot(cens(:,1)-Xmin,cens(:,2)-Ymin, 'b*')
%                  hold off
%                  disp('Press key to continue\n');
%                  w = waitforbuttonpress;
%                  close
%              end
```

Record centroids if there are more than 3 markers

```
if(length(cens)>3 & recordflag==0)
    record_i= im_i;
    recordflag=recordflag+1;
end
if (recordflag~=0)
    all_cens{im_i-record_i+1,1}=cens;
    all_cens{im_i-record_i+1,2}=length(cens);
    all_cens{im_i-record_i+1,3}=im_i;
    %x range where new markers can enter
    all_cens{im_i-record_i+1,4}(1,1)=(Xmin+w/2)-w/6;
    all_cens{im_i-record_i+1,4}(1,2)=(Xmin+w/2)+w/6;

end

im_i
cens=0;
sols=0;
eccs=0;

    end

end
```

tracking markers and linking

```
search_range=15;
for frame=2:length(all_cens)

    %directly copy for first frame
    if frame==2
        all_cens_linked1{frame,1}=all_cens{frame,1};
    else
        %look at markers in current frame
        % if a new marker is detected, its index is assumed to  be the
 same as number
```

```
        % of markers in the corresponding frame,this handles two
 markers as
        % well new_i is decremented
        n_markersi=length(all_cens{frame,1});
        new_n=n_markersi-length(all_cens_linked1{frame-1,1});
        new_i=length(all_cens_linked1{frame-1,1})+1;
        %for subsequent frames, copy the closest corresponding marker
        %look at new markers one by one
        %keep track of which markers have been linked to new frame
        for i=1:length(all_cens_linked1{frame-1,1})
            linkedi(i)=0;
        end
        %look at one marker from next frame at a time, curr_i
        for curr_i=1:length(all_cens{frame,1})
            dist=0;
            % measure distance to each of the markers in previous
 frame
            % that were linked

            for prev_i=1:length(all_cens_linked1{frame-1,1})
                % find last non zero value
                nonzero_frame=frame-1;
                while all_cens_linked1{nonzero_frame,1}(prev_i,1)==0
                    nonzero_frame=nonzero_frame-1;
                end
                %marker found in prev frame
                xdistsq=(all_cens{frame,1}(curr_i,1)-
all_cens_linked1{nonzero_frame,1}(prev_i,1))^2;
                ydistsq=(all_cens{frame,1}(curr_i,2)-
all_cens_linked1{nonzero_frame,1}(prev_i,2))^2;
                %distance to each marker copied in prev frame
                dist(prev_i)=sqrt(xdistsq+ydistsq);
            end
            [M,I]=min(dist);
            M
            %link with closest marker copied from prev frame
            if (M<search_range)
                all_cens_linked1{frame,1}(I,1:2)=all_cens{frame,1}
(curr_i,1:2);
                %indicate that the marker from previous frame has been
 linked
                linkedi(I)=1;
                % if its a new marker
            elseif (M<300)
                all_cens_linked1{frame,1}(new_i,1:2)=all_cens{frame,1}
(curr_i,1:2);
                new_i=new_i+1
            end
        end
        % after linking all markers in new frame to old frame, see if
 any
        % were not linked, then copy the same position
        %[m,n]=size(linkedi)
        for i=1:length(linkedi)
```

```
            all_cens_linked1{frame,1}(i,3)=linkedi(i);
            if(linkedi(i)==0)
                all_cens_linked1{frame,1}
(i,1:2)=all_cens_linked1{frame-1,1}(i,1:2);
            end
        end
        linkedi=0;
    end
    all_cens_linked1{frame,2}=all_cens{frame,3};
    all_cens_linked1{frame,3}=length(all_cens_linked1{frame,1});
    dist=0;
```

To plot superimposed centroids of each object in the image

```
    frame
    all_cens_linked1{frame,1}
%       if frame==600
%
       % Example input
%         X = all_cens_linked1{frame,1}(:,1);
%         Y = all_cens_linked1{frame,1}(:,2);
%         scatter(X, Y, 'filled')
%         labels = num2str((1:size(X))','%d');    %'
%         text(X, Y, labels, 'horizontal','left', 'vertical','bottom')
%         disp('Press key to continue\n');
%         w = waitforbuttonpress;
%         close
%     end

end
```

Measure the ratio of frames in which the marker is detected since first detection and filter out

```
[m,n]=size(all_cens_linked1);

for frame=3:m
    for marker=1:length(all_cens_linked1{frame,1})
        det_count(marker)=0;
        det_tot(marker)=0;
    end
end
for frame=3:m
    for marker=1:length(all_cens_linked1{frame,1})
        det_count(marker)=det_count(marker)+all_cens_linked1{frame,1}
(marker,3);
        det_tot(marker)=det_count(marker)+1;
    end
end
[m,n]=size(det_count);
```

```
for i=1:n
    det_ratio(i)=det_count(i)/det_tot(i);
end
for frame=3:length(all_cens_linked1)
    for marker=1:length(all_cens_linked1{frame,1})
        if(det_ratio(marker)>.8)
            all_cens_linked{frame,1}
(marker,1:3)=all_cens_linked1{frame,1}(marker,1:3);
        end
    end
end
```

Plot paths

```
j=2;
x=0;
y=0;

for i=300:length(all_cens_linked)

    x(i)=all_cens_linked{i,1}(j,1);

    y(i)=all_cens_linked{i,1}(j,2);

end
scatter(x,y);
```

Measure distances

sort into left arm and right arm,

```
%compare the last and 5th last frame should exist
lcount=1;
rcount=1;
x=0;
for i=1:length(all_cens_linked{end-1,1})
    x(i)=all_cens_linked{end-1,1}(i,1);
    if(x(i)<Xmin_exc)
        l_marker(lcount)=i;
        lcount=lcount+1;
    elseif (x(i)>Xmax_exc)
        r_marker(rcount)=i;
        rcount=rcount+1;
    end
end
```

Sort into positions in each arm

```
%check last frame, should exist
l_mark=all_cens_linked{end,1}(l_marker(1:end),1);
```

```
r_mark=all_cens_linked{end,1}(r_marker(1:end),1);
[L,Il]=sort(l_mark,'ascend');
[R,Ir]=sort(r_mark,'descend');
```

Measure distance through test

```
noisycount=1;
for i=2:length(all_cens_linked)
    found_markers=length(all_cens_linked{i,1});
    %run pairs through markers in left arm
    for lj=1:length(Il)-1
        %check if this pair of markers exists in this frame
        if (l_marker(Il(lj))<=found_markers && l_marker(Il(lj
+1))<=found_markers)
            xdistsq=(all_cens_linked{i,1}(l_marker(Il(lj)),1)-
all_cens_linked{i,1}(l_marker(Il(lj+1)),1))^2;
            ydistsq=(all_cens_linked{i,1}(l_marker(Il(lj)),2)-
all_cens_linked{i,1}(l_marker(Il(lj+1)),2))^2;
            ldist(i,lj)=sqrt(xdistsq+ydistsq);
            %make noisy values zero
            if (ldist(i,lj)>500)
                noisy(noisycount)=i;
                ldist(i,lj)=0;
                noisycount=noisycount+1;
            end
        end
    end
    for rj=1:length(Ir)-1
        if (r_marker(Ir(rj))<=found_markers && r_marker(Ir(rj
+1))<=found_markers)
            xdistsq=(all_cens_linked{i,1}(r_marker(Ir(rj)),1)-
all_cens_linked{i,1}(r_marker(Ir(rj+1)),1))^2;
            ydistsq=(all_cens_linked{i,1}(r_marker(Ir(rj)),2)-
all_cens_linked{i,1}(r_marker(Ir(rj+1)),2))^2;
            rdist(i,rj)=sqrt(xdistsq+ydistsq);
            if (rdist(i,rj)>300)
                noisy(noisycount)=i;
                rdist(i,rj)=0;
                noisycount=noisycount+1;
            end
        end
    end
end
```

Plot length for check

```
figure
plot(ldist(:,:));
title('Distance between spans vs Frame in Left Arm')
xlabel('Frame After Start of Recording Positions')
ylabel('Distance in pixels')
print(strcat('Leftdist_',specimen),'-dpng')
w = waitforbuttonpress;
```

```
close
figure
plot(rdist(:,:));
title('Distance between spans vs Frame in Right Arm')
xlabel('Frame After Start of Recording Positions')
ylabel('Distance in pixels')
print(strcat('Rightdist_',specimen),'-dpng')
w = waitforbuttonpress;
close
```

Stretch

```
for frame=1:length(rdist)
    for span=1:length(rdist(frame,:))
        stretchr(frame,span)=rdist(frame,span)/indist_r(span);
    end
end
for frame=1:length(ldist)
    for span=1:length(ldist(frame,:))
        stretchl(frame,span)=ldist(frame,span)/indist_l(span);
    end
end
```

Plot stretch for check

```
figure
plot(stretchr(:,:));
title('Stretch in Right Arm vs Frame')
xlabel('Frame After Start of Recording Positions')
ylabel('Stretch')
print(strcat('Rightstretch_',specimen),'-dpng')
w = waitforbuttonpress;
close
figure
plot(stretchl(:,:));
title('Stretch in Left Arm vs Frame')
xlabel('Frame After Start of Recording Positions')
ylabel('Stretch')
print(strcat('Lefttstretch_',specimen),'-dpng')
w = waitforbuttonpress;
close
```

Save to .mat

```
save('im_in.mat','im_in','im_fin')
save('stretch.mat','stretchl','stretchr')
save('spandist.mat','ldist','rdist');
```

Published with MATLAB® R2016b

APPENDIX B

CREEP AND RELAXATION

B.1 Introduction

The arterial wall is subject to dyanamic loading like pulsatile flow. It is largely accepted that arterial tissue exhibits creep under constant load and relaxation under constant strain. It is also generally observed that arterial tissue shows a fairly repeatable response under cyclic loading after a certain level of preconditioning. While studies have extensively looked into the elastic properties of the aorta wall, very few have tried to understand the time dependent response. This could help in understanding the effects of procedures like atherogenosis and balloon angioplasty. Here a step towards characterizing time dependent behavior of the arterial wall under large amplitude shear is attempted. A step shear strain of %50 is applied and help for 1000s for relaxation. For creep a torque of 4N-mm is applied and held for a period of 1000s. Samples are tested from upper and lower thoracic porcine aorta.

[19] Learoyd et al. have conducted static and dynamic measurements of the properties of the aortic wall. They followed the procedure of Bergel for both static and dynamic measurements.

For static measurements, the diameter of the vessel was recorded as the pressure was varied from 10 to 20 mm Hg. For dynamic studies, the vessels were held at a mean pressure of 100 mm Hg and oscillations of 5 to 10 mm Hg were induced. The diameter and phase difference was determined.

Phase lag and complex elastic modulus were calculated. It is noted that a simple Kelvin Voigt model was used. It was observed that there was an increase in phase

angle with increasing frequency. The findings confirmed those found by Bergel. They go on to propose that the high viscosity in femoral arteries is due to their high muscle content.

[16] Imura et al. investigated the viscoelastic properties of the human aorta in vivo by measuring the pressure-diameter relationship non invasively. They found that the in vivo and in vitro aortic wall viscosity measurements were in good agreement.

An ultrasonic displacement meter was used to determine the diameter of the wall using the time difference between echo signals. Pulsatile and mean displacements of the aortic wall were measured. Aortic pressure was also measured using a catheter tip manometer which was inserted through a sheath punctured into the femoral artery. So pressure, pulsatile diameter change, and mean diameter were all measured simultaneously.

Pressure strain modulus was obtained at different frequency components and the nonlinear elastic component was separated from the linear viscous component.

It was suggested that surrounding tissues are the reason for the discrepancy between in vivo and in vitro measurements. But this study found that no apparent differences in phase lag found and so the surrounding tissues are proposed to have a negligible effect on the viscosity.

[43] Yuj et al. characterized the mechanical properties of canine aorta based on previous experiments of the same type by Fung (1967,1972,1973). They looked into the stress-strain curves, relaxation function and creep function.

Stress-strain tests were performed on a tensile testing machine. Before testing, each specimen was subject to preconditioning. The initial values of width, length and thickness are measured before conducting the test. Relaxation tests and creep tests were also conducted.

They go on to present the results of their tests and present stress-strain relations

at a constant rate, different strain rates, relaxation function, and creep function. Comments are provided upon the large standard deviation in test results given that these are biological specimens.

[10] Gow et al. investigated the dynamic elastic moduli and viscous moduli at various locations of canine arteries. The experimental methods is discussed.

Mongrels and greyhounds were anesthetized and ventilated with a respiratory pump. Then pulsatile pressure was measured using a pressure transducer through a nylon catheter. The recording was taken for the thoracic aorta, femoral, carotid, iliac arteries, and abdominal aorta. Pulsatile diameter changes were recorded using low friction calipers. Elastic modulus was calculated from pressure change to diameter change ratio, phase difference was calculated and complex modulus was also recorded. From this dynamic elastic modulus and viscous modulus was also calculated.

[4] Azuma et al. carried out stress relaxation and stress-strain tests on circumferential and longitudinal segments from various locations of the canine aorta.

After removing the aorta and obtaining rectangular segments, they were attached to a tensile testing machine for carrying out tensile tests as well as stress relaxation tests.

An exponential relationship was found between relaxation strength and plastic deformation.

[13] [14] Holzapfel et al. presented a structural model predicting the 3 d time-dependent response of the arterial walls under different loading conditions. It is formulated within nonlinear continuum mechanics and suited for finite element formulation. The model is important because it is based on histological information and they present an automatic technique to obtain the details of the orientation of the collagen fibers in the tissue. The arterial wall is assumed to behave incompressibly. We don't go into the further details of the paper.

From the test results, graphs of the relaxation functions for each of the aortic segments were obtained. [25] Patel et al. along with Young here complete a similar study except in living canine specimens. There are major changes in the experimental setup and theory presented focuses more on dynamic aspects.

B.2 Initial Results

Aorta	Sample	Normal Force (N)	Thickness (mm)
1	a	0.16	1.849
1	b	0.15	1.674
1	c	0.15	1.576
2	a	0.15	1.571
2	b	0.15	1.427
2	c	0.15	1.546
3	a	0.16	1.809
3	b	0.17	1.674
3	c	0.15	1.5
4	a	0.16	1.723
4	b	0.17	1.523
4	c	0.16	1.322

Table B.1: Lower Descending Aorta Relaxation Dimensions

Aorta	Sample	Normal Force (N)	Thickness (mm)
1	a	0.15	2.155
1	b	0.15	1.757
1	c	0.17	1.614
2	a	0.16	1.573
2	b	0.16	1.64
2	c	0.15	1.69
3	a	0.16	1.599
3	b	0.15	1.411
3	c	0.16	1.645
4	a	0.17	1.618
4	b	0.16	1.553
4	c	0.16	1.58

Table B.2: Lower Descending Aorta Creep Dimensions

Aorta	Sample	Normal Force (N)	Thickness (mm)
1	a	0.16	2.067
1	b	0.16	1.895
1	c	0.15	2.572
2	a	0.15	2.216
2	b	0.16	1.804
2	c	0.15	1.652
3	a	0.16	2.09
3	b	0.16	1.957
3	c	0.16	1.813
4	a	0.17	1.878
4	b	0.16	2.064
4	c	0.16	1.647

Table B.4: Upper Descending Aorta Creep Dimensions

Aorta	Sample	Normal Force (N)	Thickness (mm)
1	a	0.15	2.063
1	b	0.16	2.557
1	c	0.15	2.824
2	a	0.16	1.754
2	b	0.16	2.229
2	c	0.15	1.665
3	a	0.16	2.276
3	b	0.16	2.336
3	c	0.17	1.814
4	a	0.16	2.254
4	b	0.16	1.879
4	c	0.17	1.922

Table B.3: Upper Descending Aorta Relaxation Dimensions

Some representative results from creep test for the lower descending aorta sample B.1 is shown here. The results from the relaxation tests for the lower descending aorta B.2 is also found here. We can see an initial rise time that is cut off for the remaining plots. The relaxation tests for all samples tested is found in B.6 and B.5. The creep tests for all samples tested are found here as well B.4 and B.3.

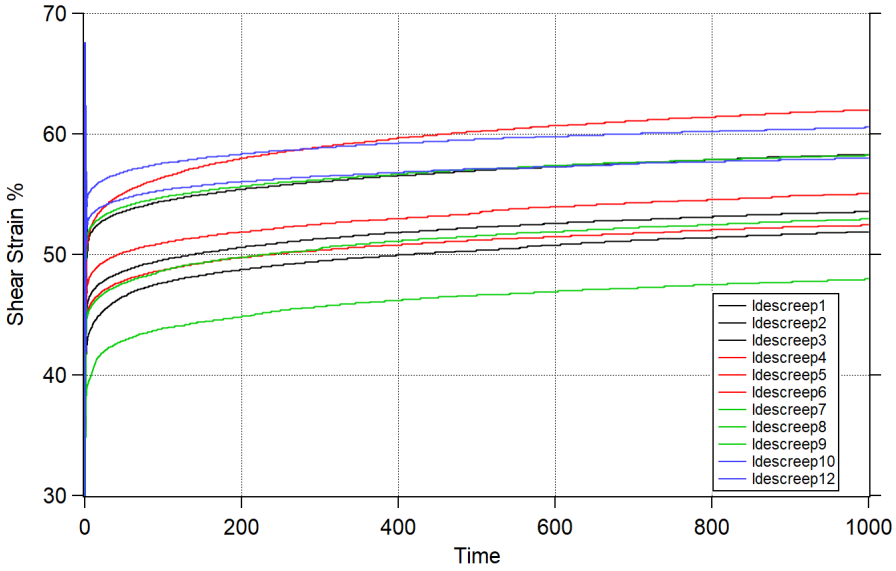

(a) Lower Descending Creep

Figure B.1: Raw Data from Experiments

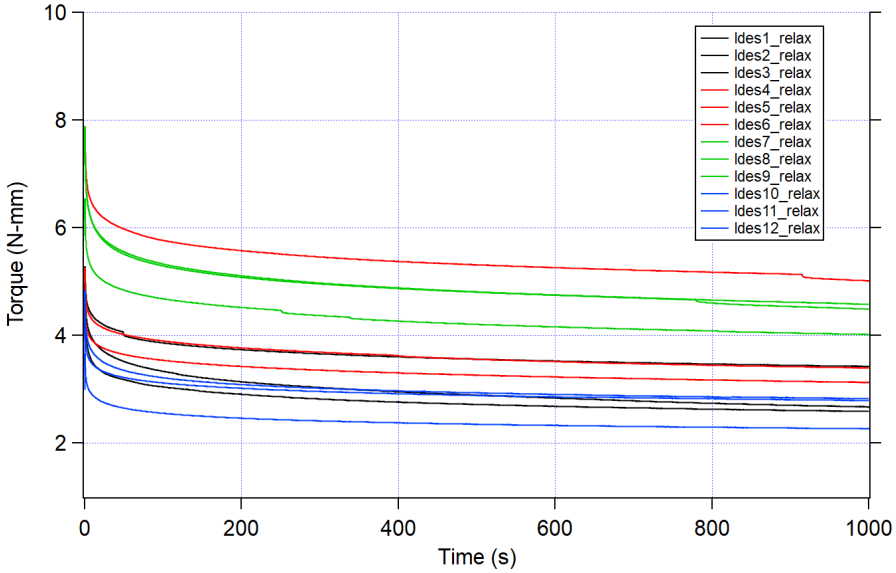

(a) Lower Descending Relaxation

Figure B.2: Raw Data from Experiments

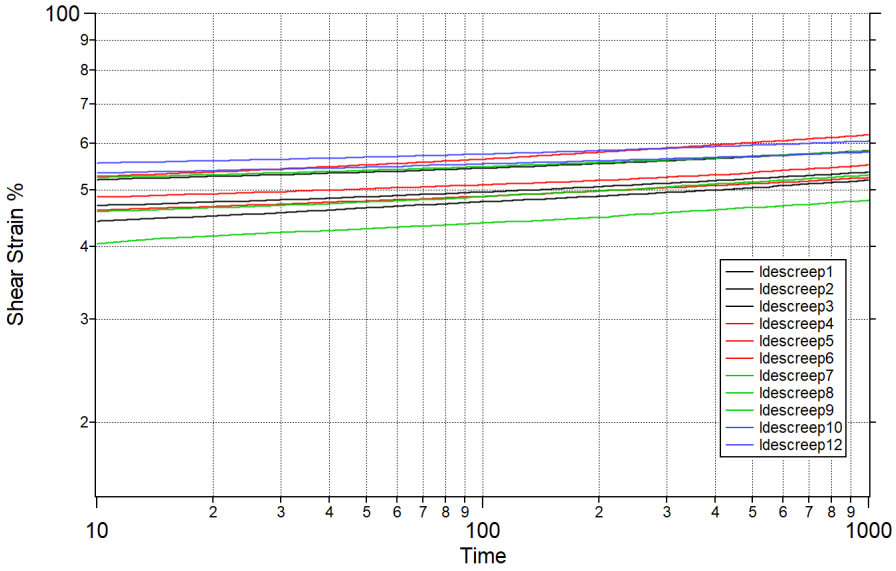

(a) Lower Descending Creep

Figure B.3: Creep under 4N-mm moment

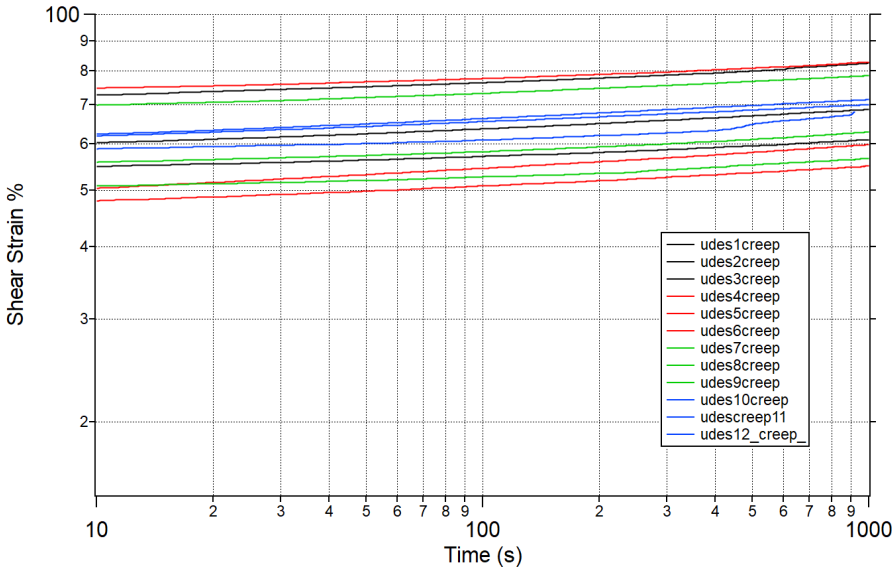

(a) Upper Descending Creep

Figure B.4: Creep under 4N-mm moment

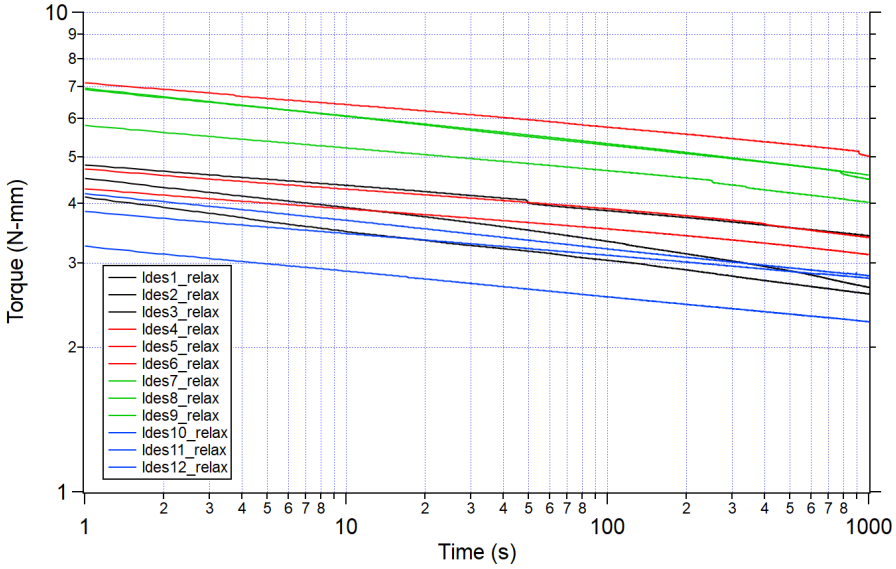

(a) Lower Descending Relaxation

Figure B.5: Relaxation with 50% shear strain

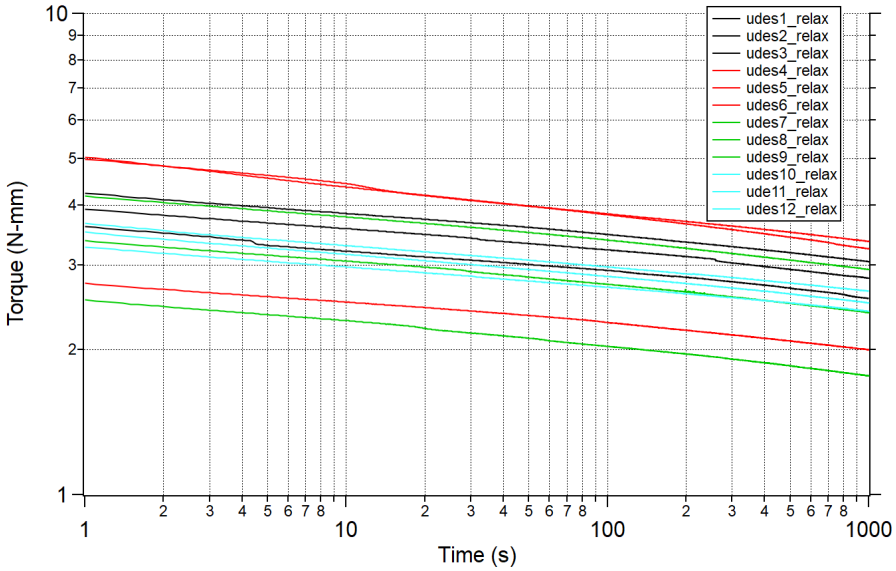

(a) Upper Descending Relaxation

Figure B.6: Relaxation with 50% shear strain

B.3 Conclusions

Many prior studies have looked into the creep and relaxation behavior in uniaxial or biaxial conditions. [44], [45] Zhang et al present an experimental approach using a biaxial tester to study relaxation and creep in elastin of porcine arterial segments. They also look into the static stress responses of bovine arterial segments.

The aorta specimen is isolated for elastin. Then, the sample measurements are taken. SEM is performed on the cross sections of tissue samples to check morphology. Histological studies are also performed to check the removal of cells in ECM, collagen and other ECM components from the isolated elastin. After the sample is prepared, it is tested by relaxation and creep tests on a biaxial tester with preconditioning.

[42] Young et al. have studied the nonlinear viscoelasticity of canine arterial segments. They imposed steps of simultaneous circumferential and longitudinal strain and measured the pressure and force to obtain relaxation functions. A theory is presented considering the aortic tissue to be incompressible and curvilinearly orthotropic and capable of large deformations.

Aortas were obtained from 7 dogs. The apparatus largely consisted of two mechanical stops, a pressure transducer, one movable leg, a tissue bath, a force gauge, and a syringe. For the tests states of strain were imposed by simultaneously stretching longitudinally and pressurizing the segment using the syringe.

Procedures like balloon angioplasty require a viscoelastic model to be studied. Experimental data on the creep and relaxatoion of the arterial wall under shear could be important to the development of models to investigate such procedures.